




Work Fluctuations in Ergotropic Heat Engines

Giovanni Chesi ^{1,*} , Chiara Macchiavello ^{1,2}  and Massimiliano Federico Sacchi ^{2,3} 

¹ National Institute for Nuclear Physics, Sezione di Pavia, Via Agostino Bassi 6, 27100 Pavia, Italy; chiara@unipv.it

² QUIT Group, Dipartimento di Fisica, Università degli Studi di Pavia, Via Agostino Bassi 6, 27100 Pavia, Italy; msacchi@unipv.it

³ CNR-Istituto di Fotonica e Nanotecnologie, Piazza Leonardo da Vinci 32, 20133 Milano, Italy

* Correspondence: giovanni.chesi@pv.infn.it

Abstract: We study the work fluctuations in ergotropic heat engines, namely two-stroke quantum Otto engines where the work stroke is designed to extract the ergotropy (the maximum amount of work by a cyclic unitary evolution) from a couple of quantum systems at canonical equilibrium at two different temperatures, whereas the heat stroke thermalizes back the systems to their respective reservoirs. We provide an exhaustive study for the case of two qutrits whose energy levels are equally spaced at two different frequencies by deriving the complete work statistics. By varying the values of temperatures and frequencies, only three kinds of optimal unitary strokes are found: the swap operator U_1 , an idle swap U_2 (where one of the qutrits is regarded as an effective qubit), and a non-trivial permutation of energy eigenstates U_3 , which indeed corresponds to the composition of the two previous unitaries, namely $U_3 = U_2U_1$. While U_1 and U_2 are Hermitian (and hence involutions), U_3 is not. This point has an impact on the thermodynamic uncertainty relations (TURs), which bound the signal-to-noise ratio of the extracted work in terms of the entropy production. In fact, we show that all TURs derived from a strong detailed fluctuation theorem are violated by the transformation U_3 .

Keywords: quantum thermodynamics; quantum heat engines; thermodynamic uncertainty relations; two-stroke Otto cycles; ergotropy



Citation: Chesi, G.; Macchiavello, C.; Sacchi, M.F. Work Fluctuations in Ergotropic Heat Engines. *Entropy* **2023**, *25*, 1528. <https://doi.org/10.3390/e25111528>

Academic Editors: Tan Van Vu and Keiji Saito

Received: 9 October 2023

Revised: 2 November 2023

Accepted: 4 November 2023

Published: 9 November 2023



Copyright: © 2023 by the authors. Licensee MDPI, Basel, Switzerland. This article is an open access article distributed under the terms and conditions of the Creative Commons Attribution (CC BY) license (<https://creativecommons.org/licenses/by/4.0/>).

1. Introduction

A quantum description of thermodynamic heat engines has lately become necessary to consider physical systems at the mesoscale and nanoscale [1–3], such as nanojunctions thermoelectrics [4], quantum dots [5], and biological [6,7] or chemical [8] systems. The optimal transport theory has also recently been embedded in a thermodynamic quantum framework [9]. At the quantum level, the fluctuations of the thermodynamic variables play a fundamental role, due to the discrete spectral structure of quantum systems.

The probability distributions of a set of thermodynamic variables $\{X_i\}$ (energy, work, heat, particles, ...) are related to the entropy production Σ through the so-called fluctuation theorems, which in general can be expressed as [10–28]

$$\frac{p(\{X_i\}, \Sigma)}{p_B(\{-X_i\}, -\Sigma)} = e^\Sigma \quad (1)$$

where p_B refers to the backward process, i.e., to the time-reversed process identified by p . For a self-contained derivation of Equation (1) and its meaning in our context see Appendix A and Equation (A22). There, a thermodynamical cycle is described by a set of stochastic trajectories which correctly reproduce the mean values $\{\langle X_i \rangle, \langle \Sigma \rangle\}$ of all variables $\{X_i\}, \Sigma$ by an average over all possible trajectories. Through the relation in Equation (1), the symmetries of the processes set relevant constraints on the statistics of the variables $\{X_i\}$. Another class of relations that connects the statistical properties of

mesoscopic and nanoscopic systems to the entropy production is given by the so-called thermodynamic uncertainty relations (TURs) [9,26,29–39]. It has been shown that there is a strong connection between fluctuation theorems and TURs, i.e., every fluctuation theorem implies a specific TUR [32]. Note that the converse does not hold: it was recently found in Ref. [38] a TUR that does not stem from any fluctuation theorem.

Thermodynamic engines that admit a straightforward quantum description are the ones based on the Otto cycle [28,35,36,40–50] since the work and heat exchanged are unambiguously identified by their respective distinct strokes. The case considered in this paper, namely a two-stroke Otto cycle, is outlined in Figure 1, where the working fluid is represented by two qutrits.

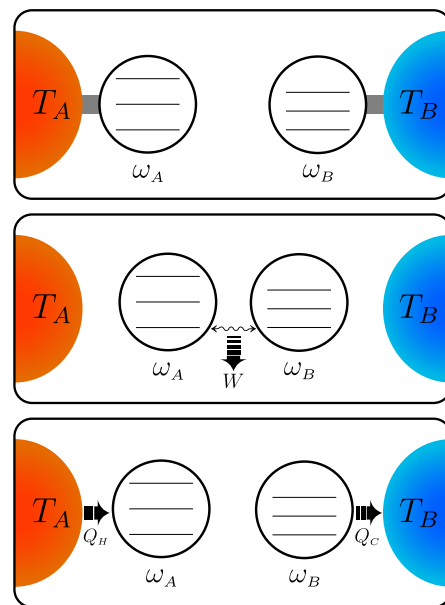


Figure 1. Scheme of a quantum thermodynamic engine based on the two-stroke Otto cycle with two qutrits as working fluid. In the first stage, the qutrits A and B with frequency ω_A and ω_B are at thermal equilibrium with the corresponding baths at temperature T_A and T_B , respectively, with $T_A > T_B$. In the second stage, the two systems are isolated and allowed to interact through a unitary evolution extracting work W . Finally, in the last stage, the systems A and B are allowed to relax to the corresponding thermal baths, implying that A absorbs the heat Q_H and B releases the heat Q_C , thus restoring the initial condition.

In the case of an engine based on a two-stroke Otto cycle, the full probability distribution of work and heat has been retrieved for two qudits [35] and for two bosonic modes [36] as working fluids, where the transformation for the work extraction is the unitary partial-swap interaction. The two-stroke Otto engine is particularly interesting with respect to its well-known four-stroke version because it allows the extraction of the maximum amount of work in the adiabatic step of the cycle by a single unitary operation, the so-called ergotropy [51–57]. Note that the extraction of the ergotropy necessarily also depends on the transformation that couples the systems. We show here that if the systems are qudits with dimensions larger than two, unitary evolutions different from the swap interaction can increase the extracted work.

We define a procedure for determining the unitary interaction that provides the maximum work from two multilevel systems A and B for a given choice of the relevant parameters, i.e., the frequency gaps ω_A and ω_B of the qudits and the temperatures T_A and T_B of the reservoirs. Then we take the specific case of a working fluid described by two qutrits and classify all the transformations that extract the ergotropy. Specifically, we find three different kinds of optimal unitary strokes: the swap operator U_1 , an idle swap U_2 (where one of the qutrits is regarded as an effective qubit), and a non-trivial permutation

U_3 given by a composition of the two previous unitaries, namely $U_3 = U_2U_1$. Each transformation extracts the ergotropy from a different regime defined by the frequency gaps ω_A and ω_B of the two qutrits and by the temperatures T_A and T_B of the baths. By deriving the characteristic function of work and heat, we evaluate the work statistics and the entropy production for every case. Note that a complete description of a quantum ergotropic heat engine and of the procedure for determining the work statistics is detailed in Appendix A. Then, we focus on the trade-off between ergotropy extraction and relative fluctuations $\text{var}(W)/\langle W \rangle^2$, i.e., the inverse of the signal-to-noise ratio (SNR). The evaluation of the fluctuations allows us to establish the relation between the variance of the work and the mean entropy production in terms of the TURs. A standard reference TUR bounds the fluctuations with the inverse of the entropy production as follows [29]

$$\frac{\text{var}(W)}{\langle W \rangle^2} \geq \frac{2}{\langle \Sigma \rangle}. \quad (2)$$

We show that all three ergotropic transformations violate this TUR. Moreover, U_3 is proved to beat all the TURs derived by the strong fluctuation theorem where the forward and backward processes in Equation (1) are related by the same condition $p_B(\{X_i\}, \Sigma) = p(\{X_i\}, \Sigma)$.

This paper is structured as follows. In Section 2, we define the procedure for determining the transformations extracting the ergotropy in the case where the working fluid is described by two qudits with generic dimensions d_A and d_B . Then, in Section 3, we apply our procedure to the case of two qutrits. In particular, in Section 3.1, we classify all the transformations extracting the ergotropy and their properties. In Section 3.2, we evaluate the maximum work extracted by each transformation in terms of the frequency gaps and the temperatures. In Section 3.3, we study the mean entropy production related to each interaction. In Section 3.4, we derive the work distributions. Finally, in Section 3.5, we find the relative fluctuations of work, compare the corresponding SNR to the bounds provided by the most relevant TURs, and discuss the assumptions required for these TURs to hold. In Section 4, we draw our conclusions.

2. Materials and Methods

In this work, we fix the Planck and Boltzmann constants to natural units, i.e., $\hbar = k_B = 1$. We consider two qudits A and B in a product of Gibbs states, i.e.,

$$\rho_0 = \frac{e^{-\beta_A H_A}}{Z_A} \otimes \frac{e^{-\beta_B H_B}}{Z_B} \quad (3)$$

where $H_X = \omega_X \sum_{n=0}^{d_X-1} n|n\rangle\langle n|$ is the Hamiltonian of the system $X = A, B$, each one with equally-spaced energy levels, and $Z_X = \text{Tr}[e^{-\beta_X H_X}]$ denotes the corresponding partition function, and $\beta_X = T_X^{-1}$ the inverse temperature. The number states $|n\rangle$ in the expansion of the Hamiltonians are eigenstates of the occupation number $n_X \equiv H_X/\omega_X$. Without loss of generality, we fix $T_A > T_B$.

We use the state in Equation (3) as the input to a two-stroke Otto engine. As depicted in Figure 1, the process starts with the two qudits in thermal equilibrium with their baths, at temperature T_A and T_B . Afterwards, the two qudits are isolated from their baths and we make them interact through a unitary evolution in order to extract the ergotropy. The procedure for the ergotropy extraction will be detailed in the following. Once the work has been extracted through the interaction, the two qudits are decoupled from each other and then reset to their equilibrium states, namely as in Equation (3), by re-connecting them to their thermal baths via a weak-coupling and energy-preserving interaction. In this way, no work contribution comes from the on-off interaction of the systems with the reservoirs [45,47,58]. The sequential repetition of this process leads to our two-stroke cyclic engine.

We fix the convention of positive work for the extraction from the system and positive heat for the absorption from the reservoirs. Then, in each cycle the average energy change in system A due to the unitary stroke corresponds to the average heat released by the hot reservoir A , namely $\langle Q_H \rangle = -\langle \Delta E_A \rangle$. Similarly, for the cold reservoir, $\langle Q_C \rangle = -\langle \Delta E_B \rangle$, and, for the first law of thermodynamics, the average work is given by $\langle W \rangle = \langle Q_H \rangle + \langle Q_C \rangle = -\langle \Delta E_A \rangle - \langle \Delta E_B \rangle$. Correspondingly, the average entropy production reads $\langle \Sigma \rangle = -\beta_A \langle Q_H \rangle - \beta_B \langle Q_C \rangle = (\beta_A - \beta_B) \langle \Delta E_A \rangle - \beta_B \langle W \rangle$. Our goal is the investigation of an ergotropic heat engine based on the two-qudit system described above, i.e., an engine extracting the maximum work by exploiting the difference in frequency and temperature between the systems A and B . In other words, we are looking for the unitary transformations U mapping the input ρ_0 into a state $\rho = U\rho_0U^\dagger$ such that the average extracted work is maximized, i.e.,

$$\langle W \rangle = \max_U \{ \text{Tr}[\rho_0 H] - \text{Tr}[\rho H] \} \tag{4}$$

where $H = H_A \otimes \mathbb{I}_B + \mathbb{I}_A \otimes H_B$ is the Hamiltonian of the system. The evolution that extracts the ergotropy was identified in Ref. [51] as the one minimizing the final energy $\text{Tr}[\rho H]$. In the present case, where the initial state ρ_0 has no coherence, namely, it is diagonal in the energy basis, the ergotropic evolution is the transformation that permutes the eigenstates of the input state so that the magnitude order of the energy levels is reversed with respect to the corresponding occupation fractions. More explicitly, if we take the occupation fractions of the system $e^{-(n\beta_A\omega_A + m\beta_B\omega_B)} / (Z_A Z_B)$ in descending order, the transformation permutes the related eigenstates to set the corresponding energy levels in ascending order. If the input state already displays this configuration, then the state is called passive and no transformation can extract work. In summary, since unitary transformations preserve the spectrum, the ergotropy is extracted by reversing all possible population inversion with respect to the energy levels. In the following, we provide a re-visited analysis of the first-level maximization strategy developed in Ref. [52].

The procedure of ergotropy extraction can be formalized in a compact way for two subsystems A and B of dimension d_A and d_B as follows. We consider two different permutations P_E and P_ρ of the energy eigenstates with respect to their lexicographic order. The permutation P_E sorts them so that the corresponding eigenvalues are set in ascending order, i.e.,

$$P_E H P_E^\dagger = P_E \left(\sum_{j=0}^{d_A-1} \sum_{k=0}^{d_B-1} (E_j + E_k) |jk\rangle \langle jk| \right) P_E^\dagger = \sum_{l=0}^{d_A d_B - 1} \tilde{E}_l |l\rangle \langle l| \equiv H^\uparrow \tag{5}$$

where the vector of eigenvalues $\tilde{\mathbf{E}} = \{\tilde{E}_l\}_{l=0}^{d_A d_B - 1}$ satisfies $\tilde{E}_l < \tilde{E}_{l+1} \forall l \in [0, d_A d_B - 1)$. Similarly, the permutation P_ρ rearranges the occupation numbers of the initial state in descending order, namely,

$$P_\rho \rho_0 P_\rho^\dagger = P_\rho \left(\sum_{l=0}^{d_A d_B - 1} r_l |l\rangle \langle l| \right) P_\rho^\dagger = \sum_{l=0}^{d_A d_B - 1} \tilde{r}_l |l\rangle \langle l| \equiv \rho_0^\downarrow \tag{6}$$

and $\tilde{\mathbf{r}} = \{\tilde{r}_l\}_{l=0}^{d_A d_B - 1}$ is such that $\tilde{r}_{l+1} < \tilde{r}_l \forall l \in [0, d_A d_B - 1)$. Then, we can straightforwardly find the transformation that minimizes the final energy from

$$\begin{aligned} \text{Tr}[\rho H] &= \text{Tr}[U\rho_0U^\dagger H] = \text{Tr}[\rho_0^\downarrow H^\uparrow] = \text{Tr}[P_\rho \rho_0 P_\rho^\dagger P_E H P_E^\dagger] \\ &= \text{Tr}[P_E^\dagger P_\rho P_\rho^\dagger P_E H] \end{aligned} \tag{7}$$

implying that the ergotropic transformation can be expressed as

$$U = P_E^\dagger P_\rho. \tag{8}$$

For instance, take two qubits in a Gibbs state

$$\rho_0 = \frac{1}{Z_A Z_B} \sum_{n,m=0}^1 e^{-n\beta_A \omega_A - m\beta_B \omega_B} |nm\rangle\langle nm|. \tag{9}$$

Then, the energies pertaining to the levels $|10\rangle\langle 10|$ and $|01\rangle\langle 01|$ are ω_A and ω_B , respectively, while the related occupation fractions are $Z_A^{-1} Z_B^{-1} e^{-\beta_A \omega_A}$ and $Z_A^{-1} Z_B^{-1} e^{-\beta_B \omega_B}$. If we have $\omega_A > \omega_B$ and $\beta_A \omega_A < \beta_B \omega_B$ or the symmetric case where both the order relations are reversed, the transformation that swaps $|10\rangle\langle 10|$ with $|01\rangle\langle 01|$, namely $U = U^\dagger = |00\rangle\langle 00| + |11\rangle\langle 11| + |01\rangle\langle 10| + |10\rangle\langle 01|$, extracts the ergotropy. This result appears immediately if we consider the permutation matrices P_E and P_ρ , which in this case read

$$\begin{aligned} P_E &= \theta(\omega_A - \omega_B)\mathbb{I} + \theta(\omega_B - \omega_A)U \\ P_\rho &= \theta(\beta_A \omega_A - \beta_B \omega_B)\mathbb{I} + \theta(\beta_B \omega_B - \beta_A \omega_A)U \end{aligned} \tag{10}$$

where $\theta(x)$ is the Heaviside function. The operator $P_E^\dagger P_\rho$ promptly identifies the ergotropic transformations and the corresponding ergotropic regimes, since

$$\begin{aligned} P_E^\dagger P_\rho &= [\theta(\omega_A - \omega_B)\theta(\beta_A \omega_A - \beta_B \omega_B) + \theta(\omega_B - \omega_A)\theta(\beta_B \omega_B - \beta_A \omega_A)]\mathbb{I} + \\ & [\theta(\omega_A - \omega_B)\theta(\beta_B \omega_B - \beta_A \omega_A) + \theta(\omega_B - \omega_A)\theta(\beta_A \omega_A - \beta_B \omega_B)]U. \end{aligned} \tag{11}$$

This simple example shows how the extraction of the ergotropy is entirely determined by the order relations between the parameters. In particular, the initial state of an equally-spaced two-qudit engine is described for any dimension of the qudits by a first partial order over the frequencies ω and a second one over the products $\beta\omega$. These order relations identify four basic partially ordered sets (posets). In the two-qubit example, the ergotropy can only be extracted if the initial state belongs to $\Omega \equiv \{\omega_A > \omega_B \wedge \beta_A \omega_A < \beta_B \omega_B\}$ or $\bar{\Omega}$, where the bar denotes the same poset with A and B switched. The states belonging to the remaining two sets are passive.

The description in terms of posets becomes more complex in higher dimensions. For a state as in Equation (3), the ordering procedure for the ergotropy extraction needs to establish if $k\omega_A > j\omega_B$ and if $k\beta_A \omega_A > j\beta_B \omega_B$ for every pair of natural numbers $k \in [0, d_A)$ and $j \in [0, d_B)$.

Even if the simplest non-trivial case would be a system made of a qubit and a qutrit, here, as mentioned above, we consider a two-qutrit system, so that we can use the results for the two-stroke swap Otto engine with two qudits with equal dimensions studied in Ref. [35] as a benchmark. In this scenario, each of the four basic posets mentioned above is further partitioned in four subsets, defined by the order relations $0 < y_{X_1} < y_{X_2}/2$ and $y_{X_2}/2 < y_{X_1} < y_{X_2}$, with $y = \omega$ or $\beta\omega$ and $X_1 \neq X_2$ may be A or B . The total number of posets determining the regimes for the ergotropy extraction is then sixteen. We expect some of them to be passive regimes, i.e., the input state defined by those parameters is passive. As for the others, we will show that a specific transformation can extract the ergotropy from different regimes, as we noted for the two-qubit case with the swap in the regimes Ω and $\bar{\Omega}$.

3. Results

3.1. Ergotropic Transformations

As mentioned above, we can jointly classify all the ergotropic transformations U and the corresponding ergotropic regimes by inspecting the permutations P_E and P_ρ .

In the two-qutrit case we have four posets identified by ω_A and ω_B for P_E , and four identified by $\beta_A \omega_A$ and $\beta_B \omega_B$ for P_ρ . We find different permutations P_E and P_ρ for each of the corresponding four posets, i.e., four distinct transformations. We show them associated with the corresponding poset in Figure 2. Note that, for what concerns P_ρ , we have to

distinguish three inequivalent cases identified by the relative position of points on the ω_B axis according to the value of the ratio β_A/β_B .

In summary, P_E and P_ρ are simply the identity I (i.e., no reordering is needed) for $\omega_A < 2\omega_B$ and $\beta_A\omega_A < 2\beta_B\omega_B$, respectively. For $\omega_B > 2\omega_A$ and $\beta_B\omega_B > 2\beta_A\omega_A$, both P_E and P_ρ are given by the swap U_1 , namely

$$U_1 = U_1^\dagger = |00\rangle\langle 00| + |11\rangle\langle 11| + |22\rangle\langle 22| + |01\rangle\langle 10| + |10\rangle\langle 01| + |02\rangle\langle 20| + |20\rangle\langle 02| + |12\rangle\langle 21| + |21\rangle\langle 12|, \tag{12}$$

or, equivalently, $U_1 = (24)(37)(68)$, using the cycle notation and the lexicographic ordering where the elements of the cycles are related to the kets as $|nm\rangle \rightarrow 3n + m + 1$.

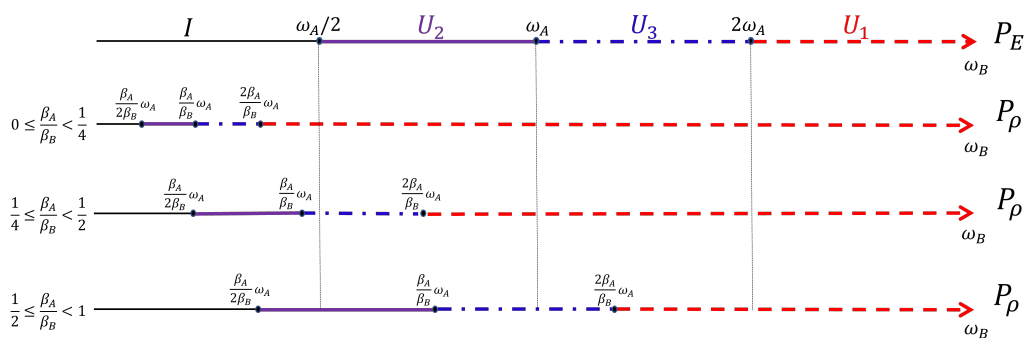


Figure 2. Scheme of the transformations realizing the permutations P_E and P_ρ in the different regimes identified by ω in the former case and by $\beta\omega$ in the latter. We show these regimes by fixing ω_A and the three inequivalent cases for the temperature ratio β_A/β_B and studying P_E and P_ρ for increasing ω_B . As ω_B increases, we find that both the permutations are given by the identity (black thin line), U_2 (purple thick line), U_3 (blue dotdashed line), and the swap U_1 (red dashed line).

For $\omega_B \in [\omega_A/2, \omega_A]$ and $\beta_B\omega_B \in [\beta_A\omega_A/2, \beta_A\omega_A]$, both P_E and P_ρ are given by

$$U_2 = U_2^\dagger = |00\rangle\langle 00| + |11\rangle\langle 11| + |22\rangle\langle 22| + |01\rangle\langle 01| + |21\rangle\langle 21| + |10\rangle\langle 02| + |02\rangle\langle 10| + |20\rangle\langle 12| + |12\rangle\langle 20| = (34)(67). \tag{13}$$

Finally, for $\omega_B \in [\omega_A, 2\omega_A]$ and $\beta_B\omega_B \in [\beta_A\omega_A, 2\beta_A\omega_A]$, both P_E and P_ρ are given by

$$U_3 = |00\rangle\langle 00| + |11\rangle\langle 11| + |22\rangle\langle 22| + |01\rangle\langle 10| + |10\rangle\langle 20| + |20\rangle\langle 21| + |21\rangle\langle 12| + |12\rangle\langle 02| + |02\rangle\langle 01| = (236874). \tag{14}$$

We notice that U_2 and U_3 are not invariant under swap symmetry. In particular, $\tilde{U}_2 \equiv U_1U_2U_1 = U_1U_3$ reads

$$\tilde{U}_2 = \tilde{U}_2^\dagger = |00\rangle\langle 00| + |11\rangle\langle 11| + |22\rangle\langle 22| + |10\rangle\langle 10| + |12\rangle\langle 12| + |01\rangle\langle 20| + |20\rangle\langle 01| + |02\rangle\langle 21| + |21\rangle\langle 02| = (27)(38), \tag{15}$$

while

$$\tilde{U}_3 \equiv U_1U_3U_1 = U_3^{-1} = U_3^\dagger. \tag{16}$$

The unitary operators U_1 , U_2 , and \tilde{U}_2 are also Hermitian and hence self-inverse. Notice also that

$$U_3 = U_1\tilde{U}_2 = U_2U_1, \tag{17}$$

and, similarly, $\tilde{U}_3 = U_1U_2 = \tilde{U}_2U_1$.

The product $P_E^\dagger P_\rho$ together with the composition rules for U_1 , U_2 and U_3 explored above allows to find the ergotropic transformations for each ergotropic regime identified by combining an ω poset with a $\beta\omega$ poset. In particular, we remark that the ergotropic transformations resulting from the product $P_E^\dagger P_\rho$ must be again U_1 , U_2 , \tilde{U}_2 and U_3 . There are

five overall, considering the identity too, which pertains to initial passive states. We provide a direct visualization of the landscape of ergotropic transformations in Figures 3–5. Having set $\beta_A < \beta_B$, each figure is linked to a different regime for the ratio β_A/β_B . As outlined in Figure 2, we can identify three distinct ranges of β_A/β_B with two critical values, namely $1/4$ and $1/2$. For each case, we show the ergotropic transformation related to each poset. In particular, we set $\beta_A/\beta_B = 1/16$ in Figure 3, $\beta_A/\beta_B = 5/16$ in Figure 4 and $\beta_A/\beta_B = 9/16$ in Figure 5. Firstly, we observe that in the first two cases, all the transformations found above appear (except \tilde{U}_3 , which pertains to the regime $T_A < T_B$). In the case of Figure 5, U_3 is never present and the number of passive regimes becomes four. Notice that in the region $0 < \beta_A/\beta_B < 1/4$, it is possible to take the limits $\beta_A \rightarrow 0$ and $\beta_B \rightarrow \infty$. In this case, one of the passive regimes disappears and most of the parameter region is dominated by the swap. On the contrary, approaching the critical point $\beta_A/\beta_B = 1/4$ we see that the region where the swap extracts the ergotropy shrinks until it vanishes at the critical point. In the second case, in Figure 4, the swap plays again a role, but the passive regimes grow as well until, at the critical point $\beta_A/\beta_B = 1/2$, the ergotropic region of U_3 vanishes and is replaced for $\beta_A/\beta_B > 1/2$ by passive regimes. Of course, at $\beta_A/\beta_B = 1$, the whole frequency subset is passive.

Let us inspect more in detail the non-trivial ergotropic transformations U_1, U_2, \tilde{U}_2 and U_3 . The swap U_1 clearly commutes with the total number operator, namely

$$[U_1, n_A \otimes \mathbb{I}_B + \mathbb{I}_A \otimes n_B] = 0. \tag{18}$$

On the other hand, the evolutions U_2 and \tilde{U}_2 act asymmetrically on the two systems, since they perform a permutation of the frequency levels of ρ_0 as if the system identified by the smallest frequency gap (B when the ergotropy is extracted by U_2 and A when it is extracted by \tilde{U}_2) were a two-level system, being its intermediate level $|1\rangle$ left unaffected. Thus, we name U_2 as *idle swap*. In fact, for this asymmetry, we have $U_2 \neq \tilde{U}_2$.

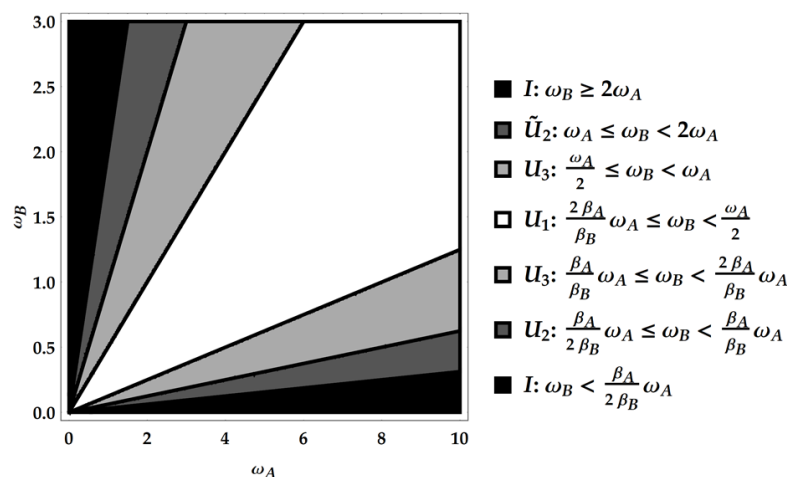


Figure 3. First case: $0 < \beta_A/\beta_B < 1/4$. Here, specifically, $\beta_A/\beta_B = 1/16$.

Differently from U_1 , the idle swaps U_2 and \tilde{U}_2 enjoy the conservation laws

$$\begin{aligned} [U_2, 2n_A \otimes \mathbb{I}_B + \mathbb{I}_A \otimes n_B] &= 0, \\ [\tilde{U}_2, n_A \otimes \mathbb{I}_B + \mathbb{I}_A \otimes 2n_B] &= 0. \end{aligned} \tag{19}$$

As for $U_3 = U_2U_1$, being the composition of the standard and the idle swap, we name it *double swap*. We noticed above that U_3 is not Hermitian. Indeed, one finds out that the double swap has multiplicative order six, namely $U_3^6 = \mathbb{I}$, as it can be inferred from the cycle notation in Equation (14). Furthermore, the double swap does not commute with any linear combination of n_A and n_B . In Appendix A, we prove that, if the transformation commutes with a linear combination of H_A and H_B , then all work and heat moments are

proportional to each other, and hence, the mean entropy production is proportional to the mean extracted work, as we will explicitly show for U_1 , U_2 and \tilde{U}_2 in the next sections.

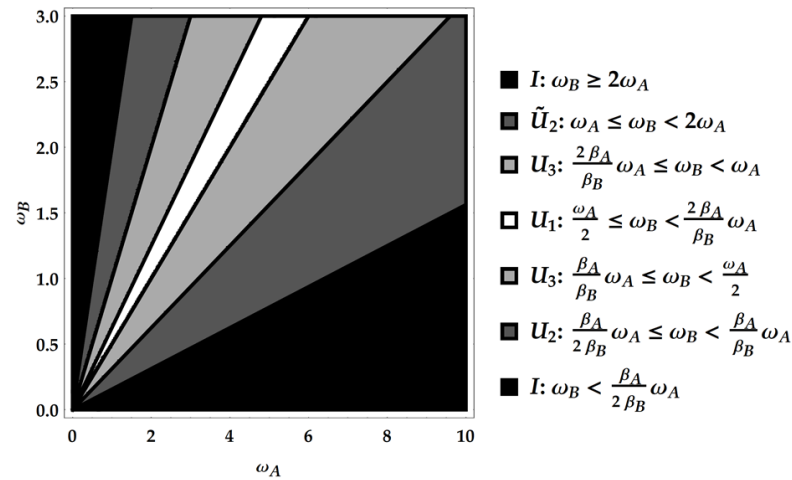


Figure 4. Second case: $1/4 < \beta_A/\beta_B < 1/2$. Here, specifically, $\beta_A/\beta_B = 5/16$.

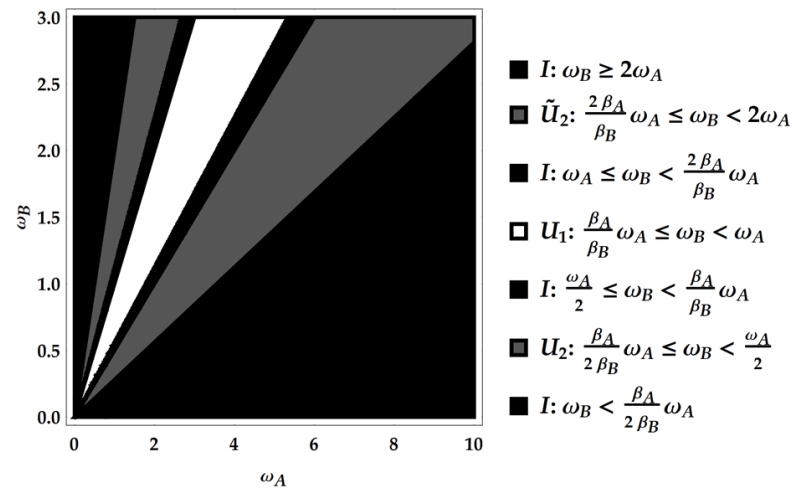


Figure 5. Third case: $1/2 < \beta_A/\beta_B < 1$. Here, specifically, $\beta_A/\beta_B = 9/16$.

3.2. Ergotropy

Now, we are ready to provide the mean work of Equation (4) extracted by each ergotropic transformation. In the case of the swap U_1 , the ergotropy can be expressed in terms of $\omega_A - \omega_B$ units and reads

$$\begin{aligned} \langle W_1 \rangle &= 2(\omega_A - \omega_B) \left[\frac{\sinh \beta_B \omega_B}{1 + 2 \cosh \beta_B \omega_B} - \frac{\sinh \beta_A \omega_A}{1 + 2 \cosh \beta_A \omega_A} \right] \\ &= 2(\omega_A - \omega_B) \frac{2 \sinh (\beta_B \omega_B - \beta_A \omega_A) + \sinh \beta_B \omega_B - \sinh \beta_A \omega_A}{(1 + 2 \cosh \beta_A \omega_A)(1 + 2 \cosh \beta_B \omega_B)}. \end{aligned} \tag{20}$$

In the case of the idle swaps U_2 and \tilde{U}_2 , we obtain

$$\langle W_2 \rangle = 2(\omega_A - 2\omega_B) \frac{\sinh \beta_B \omega_B + \sinh (\beta_B \omega_B - \beta_A \omega_A)}{(1 + 2 \cosh \beta_A \omega_A)(1 + 2 \cosh \beta_B \omega_B)} \tag{21}$$

and

$$\langle \tilde{W}_2 \rangle = 2(\omega_B - 2\omega_A) \frac{\sinh \beta_A \omega_A + \sinh (\beta_A \omega_A - \beta_B \omega_B)}{(1 + 2 \cosh \beta_A \omega_A)(1 + 2 \cosh \beta_B \omega_B)}. \tag{22}$$

Here, we recognize the action described above: the lower frequency qutrit is taken as a qubit whose gap is $2\omega_B$ for $\langle W_2 \rangle$ and $2\omega_A$ for $\langle \tilde{W}_2 \rangle$, so that the extracted work is proportional to $\omega_A - 2\omega_B$ and $\omega_B - 2\omega_A$, respectively. As expected, the work extracted from U_2 is obtained from the one extracted by \tilde{U}_2 just by swapping A with B . From Equations (20)–(22) one also verifies that

$$\frac{\langle W_1 \rangle}{1-x} = \frac{\langle W_2 \rangle}{1-2x} + \frac{\langle \tilde{W}_2 \rangle}{2-x}, \tag{23}$$

where the ratio $x \equiv \omega_B/\omega_A$ is a relevant parameter, as we will find in the following. In the case of the double swap, we have

$$\begin{aligned} \langle W_3 \rangle &= 2 \frac{\omega_A [\sinh \beta_B \omega_B + \sinh (\beta_B \omega_B - \beta_A \omega_A)] - \omega_B (\sinh \beta_A \omega_A + \sinh \beta_B \omega_B)}{(1 + 2 \cosh \beta_A \omega_A)(1 + 2 \cosh \beta_B \omega_B)} \\ &= \langle W_1 \rangle + \frac{1-2x}{x-2} \langle \tilde{W}_2 \rangle = \langle W_2 \rangle + \frac{x}{1-x} \langle W_1 \rangle. \end{aligned} \tag{24}$$

Here, we see the effects of the atypical behavior of U_3 : the extracted work is not proportional to any frequency gap. On the contrary, the frequencies ω_A and ω_B appear multiplied with different weights. Notice that for $x = 1/2$, one has $\langle W_2 \rangle = 0$ and from the second line of Equation (24) the double swap U_3 extracts the same work as U_1 , i.e., $\langle W_3 \rangle = \langle W_1 \rangle$. Instead, for $x = 1$, namely $\omega_A = \omega_B$, one has $\langle W_1 \rangle = 0$ and $\langle W_3 \rangle = \langle \tilde{W}_2 \rangle$. Finally, for $x = 2$, we have $\langle \tilde{W}_2 \rangle = 0$ and again $\langle W_3 \rangle = \langle W_1 \rangle$. In Figure 6, we represent the ergotropy extraction in the case $\beta_A/\beta_B \in (0, 1/4)$. In particular, we set the ratio $\beta_A/\beta_B = 1/16$, as in Figure 3, with $\beta_B = 10$. Note that the pretended discontinuities in the transitions between different ergotropic regions are just cusps, as it can be recognized in Figures 7–11.

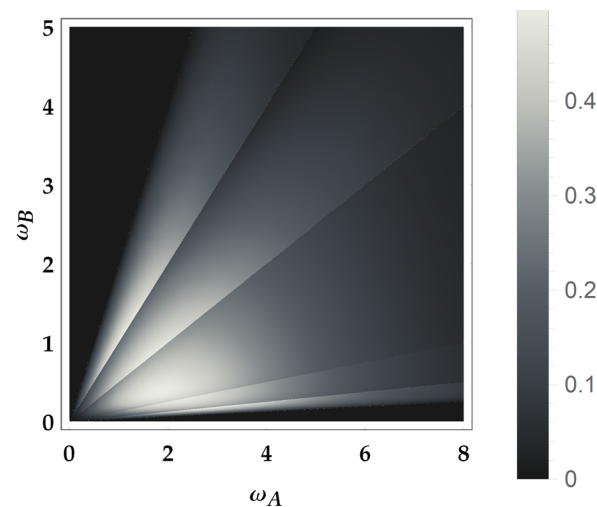


Figure 6. Ergotropy extraction in the case $0 < \beta_A/\beta_B < 1/4$. Here, $\beta_A/\beta_B = 1/16$ and $\beta_B = 10$.

In these figures, we show specific examples of ergotropy extraction as a function of ω_B , by fixing all the other parameters. Figure 7 displays the case $\beta_A/\beta_B < 1/4$, with $\beta_A/\beta_B = 1/8$. Therefore, this is not a critical point, and for varying ω_B , we span all the non-equivalent ergotropic transformations. The black dot line displays the work extracted from the standard swap U_1 so that we can see how it is outperformed by the other unitaries outside its own ergotropic regime. Moreover, the solid lines, corresponding to U_2 and \tilde{U}_2 , show that the regime of operation of an ergotropic heat engine is enlarged with respect to the swap Otto engine. In Figure 8, we consider the critical point $\beta_A/\beta_B = 1/4$, which represents the transition between the cases in Figures 3 and 4, where the ergotropic regime of the standard swap vanishes. Indeed, here we do not have any ergotropic contribution from U_1 , except for the limiting case $\omega_A = 2\omega_B$, where the work extracted coincides with the one provided by U_3 , identified by the red point. In Figure 9, we show the ergotropy as a function of ω_B for the critical point $\beta_A/\beta_B = 1/2$, which is the transition point between

the cases of Figures 4 and 5. As expected, the double swap U_3 is never required to extract the ergotropy. The maximum work is extracted by the idle swap U_2 for $\omega_B < \omega_A/2$, by the standard swap U_1 for $\omega_A/2 < \omega_B < \omega_A$ and by \tilde{U}_2 for $\omega_A < \omega_B < 2\omega_A$. For the case $\beta_A/\beta_B > 1/2$ of Figure 5, we fix in Figure 10 $\beta_A/\beta_B = 3/4$. As in the previous case, U_3 is not needed and, furthermore, there are two more passive regions. Finally, in the last example in Figure 11, we plot the ergotropy for the ideal case $\beta_A/\beta_B = 0$, by setting β_A to 0 and finite large values for ω_A and β_B . In particular, the high value of ω_A allows to see that the extracted work is large when $\omega_A - \omega_B$ is large, except for the limiting case $\omega_B \rightarrow 0$ (in such a case indeed we would have $\beta_A\omega_A = \beta_B\omega_B = 0$, implying $\langle W_1 \rangle = 0$).

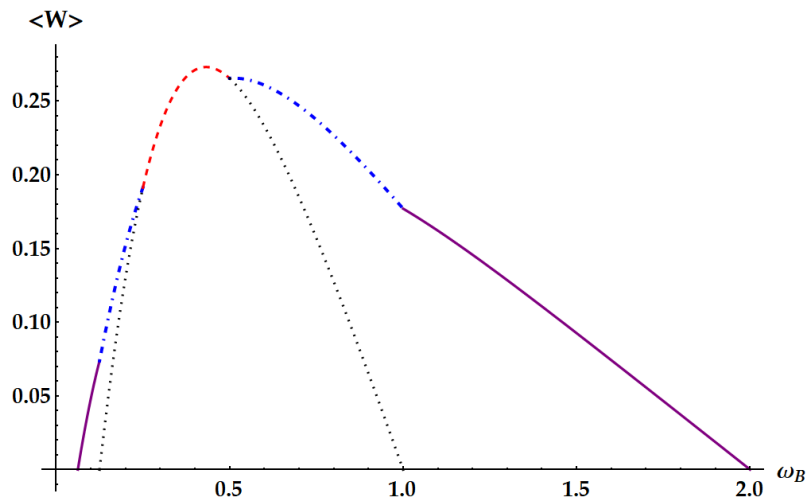


Figure 7. Ergotropy $\langle W \rangle$ as a function of ω_B in the case $\beta_A/\beta_B = 1/8$, with $\omega_A = 1$, $\beta_A = 0.5$, $\beta_B = 4$. Purple solid lines: idle swaps U_2 ($\omega_B < 1/8$) and \tilde{U}_2 ($\omega_B > 1$). Blue dot-dashed line: double swap U_3 . Red dashed line: standard swap U_1 inside the corresponding ergotropic regime. Black dotted line: standard swap for any ω_B such that the extracted work is positive.

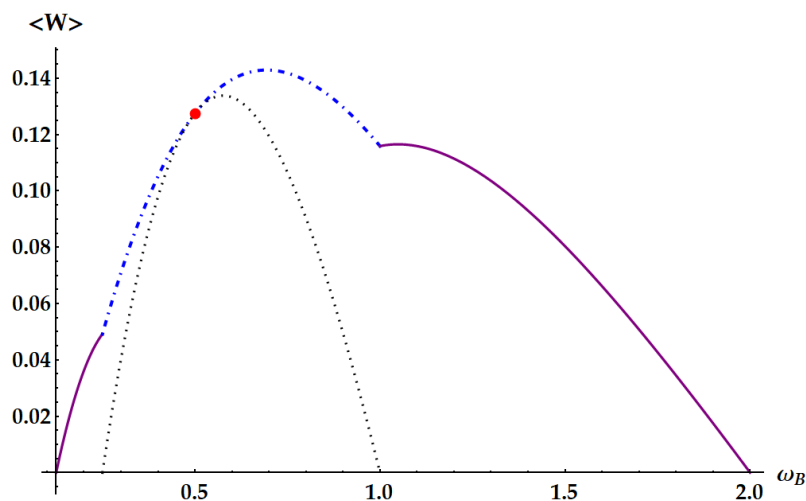


Figure 8. Ergotropy $\langle W \rangle$ as a function of ω_B at the critical point $\beta_A/\beta_B = 1/4$, with $\omega_A = 1$, $\beta_A = 0.5$, $\beta_B = 2$. The red mark identifies the tangent point where the standard swap U_1 (dotted black line) and the double swap U_3 (blue dashed-dotted line) extracts the same amount of work at $\omega_B = \omega_A/2 = 0.5$. The purple solid curves identify the ergotropy extracted by U_2 ($1/8 < \omega_B < 1/4$) and \tilde{U}_2 ($1 < \omega_B < 2$).

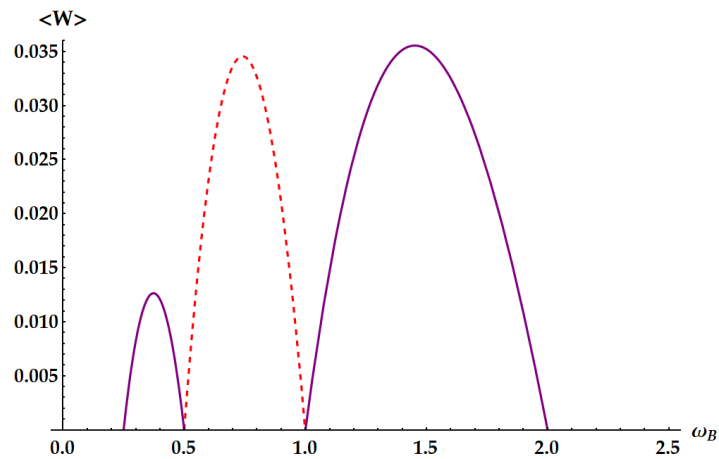


Figure 9. Ergotropy $\langle W \rangle$ as a function of ω_B in the critical case $\beta_A/\beta_B = 1/2$, with $\omega_A = 1$, $\beta_A = 0.5$, $\beta_B = 1$. Dashed red line: standard swap U_1 for $\omega_B \in [\omega_A/2, \omega_A] = [1/2, 1]$. Purple solid lines: idle swaps U_2 for $\omega_B \in [\beta_A\omega_A/2\beta_B, \omega_A/2] = [1/4, 1/2]$ and \tilde{U}_2 for $\omega_B \in [\omega_A, 2\omega_A] = [1, 2]$.

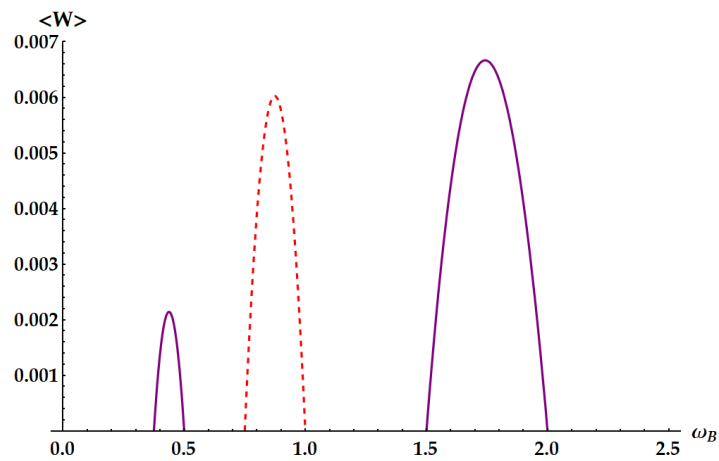


Figure 10. Ergotropy $\langle W \rangle$ as a function of ω_B in the case $\beta_A/\beta_B = 3/4$, with $\omega_A = 1$, $\beta_A = 1/2$, $\beta_B = 2/3$. Dashed red line: standard swap U_1 for $\omega_B \in [\beta_A\omega_A/\beta_B, \omega_A] = [3/4, 1]$. Purple solid lines: idle swaps U_2 for $\omega_B \in [\beta_A\omega_A/2\beta_B, \omega_A/2] = [3/8, 1/2]$ and \tilde{U}_2 for $\omega_B \in [2\beta_A\omega_A/\beta_B, 2\omega_A] = [3/2, 2]$.

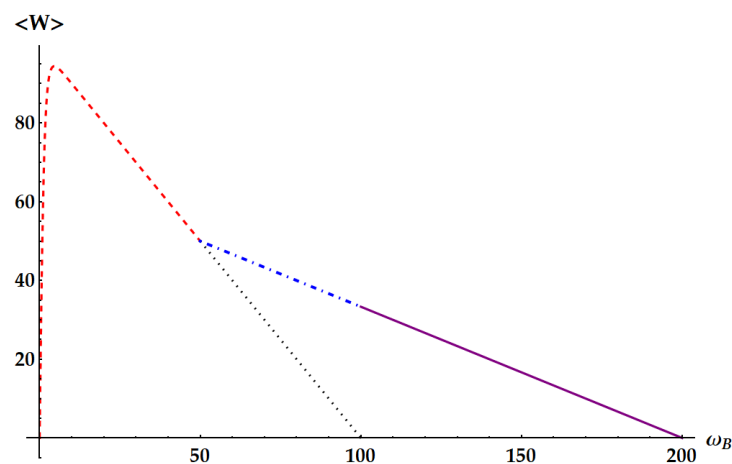


Figure 11. Ergotropy $\langle W \rangle$ as a function of ω_B in the limiting case $\beta_A/\beta_B = 0$, with $\omega_A = 100$, $\beta_A = 0$, $\beta_B = 10$. Blue dot-dashed line: double swap U_3 . Red dashed line: standard swap U_1 inside the corresponding ergotropic regime. Purple solid line: idle swap \tilde{U}_2 . Black dotted line: standard swap for any ω_B such that the extracted work is positive.

In summary, in the regime of operation of the standard swap Otto engine, i.e., $\omega_A > \omega_B \wedge \beta_A \omega_A < \beta_B \omega_B$, the work extraction may be improved by replacing the swap U_1 with the permutation U_3 . Moreover, the idle swaps U_2 and \tilde{U}_2 even allow to enlarge the range of operation of the heat engine.

3.3. Entropy Production

Let us now evaluate the mean entropy production of the quantum heat engine in order to study its relation with the work fluctuations and to explore the validity or violation of TURs. As mentioned in Section 2, the mean entropy production is given by

$$\langle \Sigma \rangle = (\beta_A - \beta_B) \langle \Delta E_A \rangle - \beta_B \langle W \rangle. \tag{25}$$

We can evaluate the moments of W and ΔE_A through the derivatives of the characteristic function, according to Equations (A27) and (A28) of Appendix A. Due to the conservation laws for U_1 , U_2 , and \tilde{U}_2 as in Equations (18) and (19), according to Equation (A34), we have

$$\langle W^l \Delta E_A^s \rangle = \alpha^s \langle W^{l+s} \rangle, \tag{26}$$

where $\alpha = \omega_A / (\omega_B - \omega_A)$ for U_1 , $\alpha = 2\omega_B / (\omega_A - 2\omega_B)$ for U_2 , and $\alpha = 2\omega_A / (\omega_B - 2\omega_A)$ for \tilde{U}_2 . Hence, the entropy production of U_1 , U_2 , and \tilde{U}_2 is proportional to their pertaining work, and one has

$$\begin{aligned} \langle \Sigma_1 \rangle &= \frac{\beta_B \omega_B - \beta_A \omega_A}{\omega_A - \omega_B} \langle W_1 \rangle, \\ \langle \Sigma_2 \rangle &= \frac{2\beta_B \omega_B - \beta_A \omega_A}{\omega_A - 2\omega_B} \langle W_2 \rangle, \\ \langle \tilde{\Sigma}_2 \rangle &= \frac{\beta_B \omega_B - 2\beta_A \omega_A}{2\omega_A - \omega_B} \langle \tilde{W}_2 \rangle, \end{aligned} \tag{27}$$

where $\langle W_1 \rangle$, $\langle W_2 \rangle$ and $\langle \tilde{W}_2 \rangle$ are given in Equations (20)–(22), respectively.

Equation (26) does not hold for U_3 , and the entropy production explicitly is given by

$$\langle \Sigma_3 \rangle = 2 \frac{\beta_B \omega_B (\sinh \beta_A \omega_A + \sinh \beta_B \omega_B) - \beta_A \omega_A [\sinh \beta_B \omega_B + \sinh (\beta_B \omega_B - \beta_A \omega_A)]}{(1 + 2 \cosh \beta_A \omega_A)(1 + 2 \cosh \beta_B \omega_B)}. \tag{28}$$

Note that in all cases the mean entropy production is positive and depends only on the ratios between frequency and temperature and not on the bare frequencies.

3.4. Work Distribution

We can now provide the explicit expression for the distribution of work $p(W)$ pertaining to each ergotropic transformation. As shown in Appendix A (see Equation (A15)), we have

$$p(W) = \sum_{n,m,l,s} p_{n,m} q(l,s|n,m) \delta(W - \omega_A(n-l) - \omega_B(m-s)) \tag{29}$$

where $p_{n,m}$ is the energy distribution of the input state, namely

$$p_{n,m} = \frac{1}{Z_A Z_B} e^{-\beta_A \omega_A n} e^{-\beta_B \omega_B m} \tag{30}$$

while $q(l,s|n,m)$ is the energy conditional distribution after the evolution U , given the input energy levels n and m , i.e.,

$$q(l,s|n,m) = |\langle l,s|U|n,m \rangle|^2. \tag{31}$$

In the case of the standard swap U_1 , the conditional distribution reads $q_1(l,s|n,m) = \delta_{l,m} \delta_{n,s}$, and hence

$$p_1(W) = \sum_{n,m=0}^2 p_{n,m} \delta(W - (n - m)\omega_A - (m - n)\omega_B), \tag{32}$$

which is a 5-point distribution. Explicitly, upon naming $k \equiv n - m$, one has

$$\begin{aligned} p_1(W = k(\omega_A - \omega_B)) &= \\ &= \frac{1}{Z_A Z_B} \frac{1 - \exp[-(k + 3)(\beta_A \omega_A + \beta_B \omega_B)]}{1 - \exp[-(\beta_A \omega_A + \beta_B \omega_B)]} e^{\beta_A \omega_A k} \quad \text{with } k \in [-2, 0) \\ &= \frac{1}{Z_A Z_B} \frac{1 - \exp[(k - 3)(\beta_A \omega_A + \beta_B \omega_B)]}{1 - \exp[-(\beta_A \omega_A + \beta_B \omega_B)]} e^{-\beta_B \omega_B k} \quad \text{with } k \in [0, 2]. \end{aligned} \tag{33}$$

A specific example is plotted in Figure 12. Equation (33) is consistent with the general result given in Ref. [35] for the work distribution in swap engines based on two qudits.

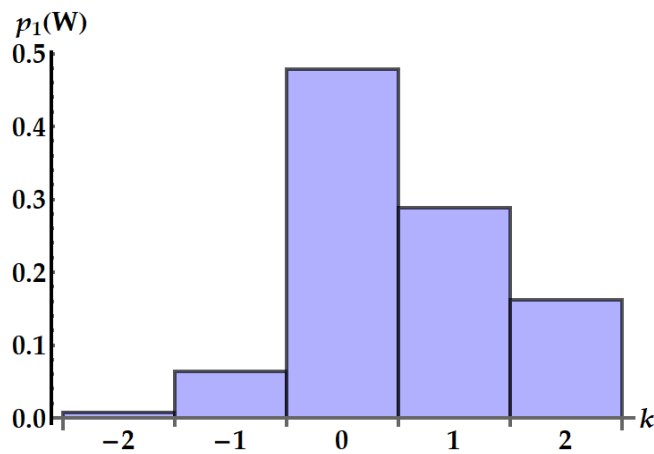


Figure 12. Distribution $p_1(W = k(\omega_A - \omega_B))$ of the work extracted by the standard swap U_1 in $\omega_A - \omega_B$ units. We set $\beta_A \omega_A = 0.5$ and $\beta_B \omega_B = 2$.

Now, we focus on the idle swap U_2 . Due to its asymmetric action on systems A and B , the conditional distribution is slightly more complicated and reads

$$q_2(l, s | n, m) = \sum_{m=0}^2 \delta_{n,m} \delta_{l,s} \delta_{s,m} + \delta_{s,2-m} (\delta_{n,m \oplus 1} + \delta_{n,m \oplus 2}) + (\delta_{l,s \oplus 1} + \delta_{l,s \oplus 2}) \tag{34}$$

where \oplus denotes the sum mod 3. Hence, one retrieves the following 3-point distribution

$$\begin{aligned} p_2(W) &= \left(\sum_{n=0}^2 p_{n,n} + p_{01} + p_{21} \right) \delta(W) + (p_{10} + p_{20}) \delta(W - \omega_A + 2\omega_B) \\ &\quad + (p_{02} + p_{12}) \delta(W + \omega_A - 2\omega_B). \end{aligned} \tag{35}$$

An example is depicted in Figure 13.

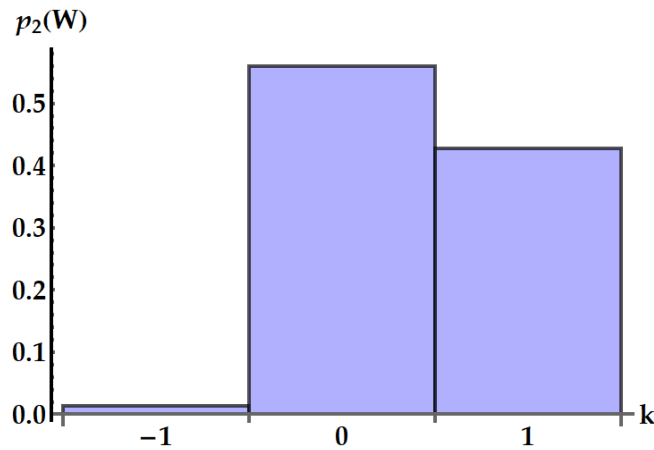


Figure 13. Distribution $p_2(W = k(2\omega_B - \omega_A))$ of the work extracted by the idle swap U_2 in $2\omega_B - \omega_A$ units. We set $\beta_A\omega_A = 0.5$ and $\beta_B\omega_B = 2$.

Similarly, in the case of \tilde{U}_2 one has

$$\tilde{p}_2(W) = \left(\sum_{n=0}^2 p_{n,n} + p_{10} + p_{12} \right) \delta(W) + (p_{01} + p_{02}) \delta(W - \omega_B + 2\omega_A) + (p_{20} + p_{21}) \delta(W + \omega_B - 2\omega_A). \tag{36}$$

Finally, since $U_3 = U_2U_1$, for the double swap we readily find

$$q_3(l, s|n, m) = q_2(l, s|m, n), \tag{37}$$

and then one obtains the following 7-point distribution

$$p_3(W) = \sum_{n=0}^2 p_{n,n} \delta(W) + p_{10} \delta(W - \omega_A + \omega_B) + p_{12} \delta(W + \omega_A - \omega_B) + p_{01} \delta(W + \omega_B) + p_{21} \delta(W - \omega_B) + p_{02} \delta(W + \omega_A) + p_{20} \delta(W - \omega_A). \tag{38}$$

A specific example is provided in Figure 14.

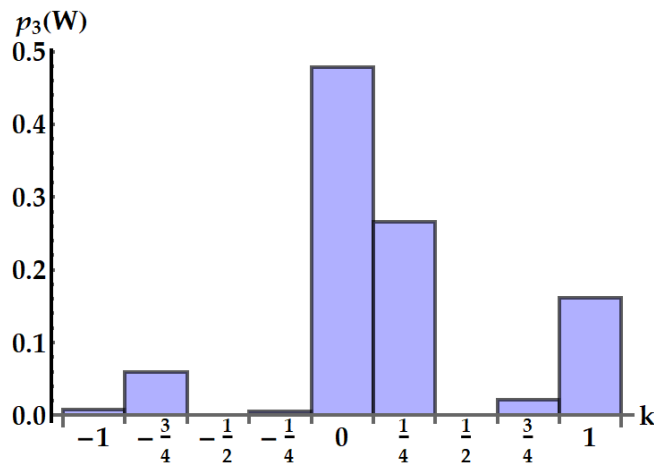


Figure 14. Distribution $p_3(W = k\omega_A)$ of the work extracted by the double swap U_3 in ω_A units in the case $\omega_B/\omega_A = 3/4$. We set $\beta_A\omega_A = 0.5$ and $\beta_B\omega_B = 2$.

3.5. Work Fluctuations and TURs

Here, we evaluate the relative fluctuations of the work extracted by the ergotropic transformations and compare them to the lower bounds identified by different thermodynamic uncertainty relations (TURs).

We can find the relative fluctuations as the ratio between the variance of the extracted work and the square of its mean value, namely $\text{var}(W)/\langle W \rangle^2 = \langle W^2 \rangle / \langle W \rangle^2 - 1$, with $\text{var}(W) = \langle W^2 \rangle - \langle W \rangle^2$. The second moment of the extracted work can be obtained from the characteristic function as in Equations (A28) and (A29), and one has

$$\begin{aligned} \langle W_k^2 \rangle = & \text{Tr}[(H_A \otimes \mathbb{I}_B + \mathbb{I}_A \otimes H_B)^2 \rho_0] + \text{Tr}[(H_A \otimes \mathbb{I}_B + \mathbb{I}_A \otimes H_B)^2 U_k \rho_0 U_k^\dagger] \\ & - 2\text{Tr}[U_k^\dagger (H_A \otimes \mathbb{I}_B + \mathbb{I}_A \otimes H_B) U_k (H_A \otimes \mathbb{I}_B + \mathbb{I}_A \otimes H_B) \rho_0]. \end{aligned} \tag{39}$$

For the standard swap U_1 one obtains

$$\begin{aligned} \frac{\text{var}(W_1)}{\langle W_1 \rangle^2} = & (1 + 2 \cosh \beta_A \omega_A)(1 + 2 \cosh \beta_B \omega_B) \\ & \times \frac{\cosh \beta_A \omega_A + \cosh \beta_B \omega_B + 4 \cosh(\beta_B \omega_B - \beta_A \omega_A)}{2[\sinh \beta_B \omega_B - \sinh \beta_A \omega_A + 2 \sinh(\beta_B \omega_B - \beta_A \omega_A)]^2} - 1 \end{aligned} \tag{40}$$

which is in agreement with the general result of the swap engine with two qudits of Ref. [35]. As expected, the fluctuations of the standard swap are invariant under swapping A and B . For the idle swap U_2 , we have

$$\frac{\text{var}(W_2)}{\langle W_2 \rangle^2} = (1 + 2 \cosh \beta_A \omega_A)(1 + 2 \cosh \beta_B \omega_B) \frac{\cosh \beta_B \omega_B + \cosh(\beta_B \omega_B - \beta_A \omega_A)}{2[\sinh \beta_B \omega_B + \sinh(\beta_B \omega_B - \beta_A \omega_A)]^2} - 1. \tag{41}$$

As for the ergotropy in Equations (21) and (22), the expression for $\text{var}(\tilde{W}_2)/\langle \tilde{W}_2 \rangle^2$ is simply obtained by exchanging A with B in Equation (41). Note that the fluctuations of both the standard and the idle swap depend only on the products $\beta\omega$.

This is not the case for the double swap U_3 , which depends also on the frequency ratio $x = \omega_B/\omega_A$ as follows

$$\begin{aligned} \frac{\text{var}(W_3)}{\langle W_3 \rangle^2} = & (1 + 2 \cosh \beta_A \omega_A)(1 + 2 \cosh \beta_B \omega_B) \\ & \times \frac{x^2 \cosh \beta_A \omega_A + (1 - x)^2 \cosh \beta_B \omega_B + \cosh(\beta_B \omega_B - \beta_A \omega_A)}{2[(1 - x) \sinh \beta_B \omega_B - x \sinh \beta_A \omega_A + \sinh(\beta_B \omega_B - \beta_A \omega_A)]^2} - 1. \end{aligned} \tag{42}$$

For all the ergotropic transformations the fluctuations are minimized in the limiting case where $\beta\omega \rightarrow 0$ for one qutrit and $\beta\omega \rightarrow \infty$ for the other one. In the case of the swap, being naturally invariant under swap symmetry, we can either set $\beta_A \omega_A$ to zero and $\beta_B \omega_B$ to infinity or the other way around. On the contrary, the case of the idle and the double swap is asymmetric and we achieve the minimum of the fluctuations for $\beta_B \omega_B \rightarrow 0 \wedge \beta_A \omega_A \rightarrow \infty$ in the case of \tilde{U}_2 and for $\beta_A \omega_A \rightarrow 0 \wedge \beta_B \omega_B \rightarrow \infty$ in the case of U_2 and U_3 . Here, we mainly focus on the transformations that extract the ergotropy in the same poset identified by the products $\beta\omega$. In particular, we choose the poset defined by $\beta_A \omega_A < \beta_B \omega_B$, where the optimal evolutions are U_1, U_2 and U_3 . In the case of the double swap U_3 , the minimization has to be performed also on the frequency ratio and the infimum is obtained for $x \rightarrow 0$. The optimization of the fluctuations over the whole span of the parameters readily provides

$$\frac{2}{3} = \inf_{\beta_A \omega_A, \beta_B \omega_B} \frac{\text{var}(W_1)}{\langle W_1 \rangle^2} > \inf_{\beta_A \omega_A, \beta_B \omega_B} \frac{\text{var}(W_2)}{\langle W_2 \rangle^2} = \inf_{\beta_A \omega_A, \beta_B \omega_B, x} \frac{\text{var}(W_3)}{\langle W_3 \rangle^2} = \frac{1}{2}. \tag{43}$$

Therefore, it turns out that U_2 and U_3 achieve smaller fluctuations than U_1 .

We now investigate if damping the noise comes together with the extraction of the ergotropy. While for U_1 this is always the case, the same is not true for U_2 and U_3 . The idle swap U_2 extracts the ergotropy for $\beta_B \omega_B < \beta_A \omega_A$, where the condition for the mini-

mization of fluctuations corresponding to U_2 does not hold. Interestingly, in that region, it is \tilde{U}_2 the ergotropy extractor. Within the ergotropic region of U_2 , we need to take $\beta_B\omega_B \rightarrow 0 \wedge \beta_A\omega_A \rightarrow \infty$, which provides $\text{var}(W_2)/\langle W_2 \rangle^2 = 2$. For U_3 , on the contrary, the condition on the ratios $\beta\omega$ for optimal fluctuations is compatible with the extraction of ergotropy, but with the additional constraint $x \geq 1/2$. The minimization over x then sets it to $1/2$, and, as discussed after Equation (24), for that frequency ratio $\langle W_3 \rangle = \langle W_1 \rangle$. To sum up, if we aim to optimize the noise inside the ergotropic regimes of each ergotropic transformation, we find that the best performance is achieved by the standard swap since

$$2 = \inf_{\beta_A\omega_A, \beta_B\omega_B} \frac{\text{var}(W_2)}{\langle W_2 \rangle^2} > \inf_{\beta_A\omega_A, \beta_B\omega_B} \frac{\text{var}(W_1)}{\langle W_1 \rangle^2} = \inf_{\beta_A\omega_A, \beta_B\omega_B, x} \frac{\text{var}(W_3)}{\langle W_3 \rangle^2} = \frac{2}{3}. \tag{44}$$

In this last regime where ergotropy extraction and minimal noise coexist, we finally note that the standard swap extracts more work than the idle and double swap. In fact, one has

$$\begin{aligned} \sup_{\omega_B} W_1(\beta_A\omega_A \rightarrow 0, \beta_B\omega_B \rightarrow \infty) &= \omega_A, \\ \sup_{\omega_B} W_2(\beta_A\omega_A \rightarrow \infty, \beta_B\omega_B \rightarrow 0) &= \frac{\omega_A}{3}, \\ \sup_{\omega_B} W_3(\beta_A\omega_A \rightarrow 0, \beta_B\omega_B \rightarrow \infty) &= \frac{\omega_A}{2}. \end{aligned} \tag{45}$$

We remark that the results found so far do imply that the standard swap is the best operation in terms of fluctuations and extracted work in the optimal limiting case $\beta_A\omega_A \rightarrow 0 \wedge \beta_B\omega_B \rightarrow \infty$, but the same does not hold for intermediate values of $\beta\omega$, as we shall see in the following.

Now, we compare the relative fluctuations of the ergotropic engine in asymptotic and non-asymptotic cases with the bounds derived from the most significant TURs. We recall that the double swap U_3 is not Hermitian. Therefore, as remarked in the Appendix after Equation (A26), U_3 could violate all the TURs based on the equivalence between forward and backward processes. On the other hand, we already know from previous works [35] that the swap itself breaks the standard TUR in Equation (2). We study in Figure 15 the violation of the standard TUR as a function of $\beta\omega$ in conditions of minimal fluctuations, independently from the ergotropic regime. Namely, in the case of U_1 (red dashed line), U_2 (purple solid line) and U_3 (blue dot-dashed line) the free variable is $\beta_B\omega_B$ with $\beta_A\omega_A \ll 1$. Just for U_3 , we also need $\omega_B/\omega_A \ll 1$. We remark that here we are not focusing on the ergotropy extraction, but only on the properties of the evolutions U_1 , U_2 , and U_3 in terms of work fluctuations. We find that all three ergotropic transformations break the standard thermodynamic uncertainty relation. In particular, the violation due to U_3 is impressive. As found in [35], when the evolution is the standard swap the relative fluctuations for the extracted work satisfies

$$\frac{\text{var}(W)}{\langle W \rangle^2} \geq \frac{2}{\langle \Sigma \rangle} - 1. \tag{46}$$

The variation of Equation (46) from the standard TUR explains the slight violation found in Figure 15, where the lower bound from the standard TUR is displayed as a black dotted line. Similarly to U_1 , also U_2 and \tilde{U}_2 satisfy Equation (46). In fact,

$$\frac{\langle W_2^2 \rangle}{\langle W_2 \rangle^2} = \frac{f(\beta_A\omega_A, \beta_B\omega_B)}{\langle \Sigma_2 \rangle} \tag{47}$$

where

$$f(x, y) \equiv (2y - x) \frac{\cosh y + \cosh(y - x)}{\sinh y + \sinh(y - x)}, \tag{48}$$

which satisfies

$$f(x, y) \geq 2 \quad \forall x, y \geq 0. \tag{49}$$

The fluctuations originated from U_3 , instead, can break the TUR in Equation (46). Such violation stems from the asymmetry of the process described by U_3 , which is not Hermitian. Indeed, we note that a necessary condition for the TURs in Equations (2) and (46) to hold is the equivalence between forward and backward process, i.e., $p_B(W, \Delta E_A) = p(W, \Delta E_A)$. Moreover, note that the double swap is the only transformation whose fluctuations depend also on the frequency ratio while leaving the mean entropy as a function of just $\beta_A \omega_A$ and $\beta_B \omega_B$. Therefore, in this case, we can optimize over a third parameter without changing the lower bound of the TUR.

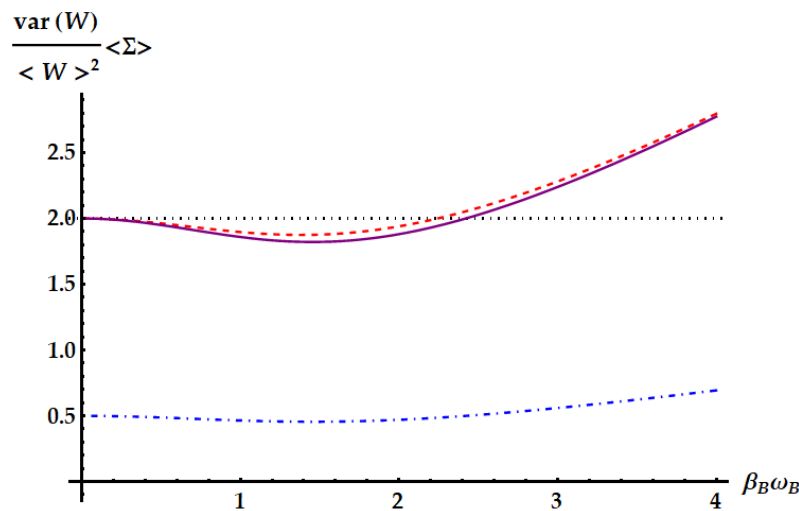


Figure 15. Product of the relative fluctuations with the mean entropy production, which is lower bounded by 2 (black dotted line) in the standard TUR of Equation (2) and by a function of the mean entropy in Equation (50). We set $\beta_A \omega_A = 10^{-3}$. The plot shows the violations due to the standard swap U_1 (red dashed line), the idle swap U_2 (solid purple line) and the double swap U_3 (blue dot-dashed line) as a function of $\beta_B \omega_B$.

The violation of the TUR in Equation (46) by U_3 can also be found in realistic cases, i.e., even if we do not set the parameters to the values minimizing the fluctuations. Actually, these cases are the most relevant to be considered, not only because closer to experimental applications but especially because they keep into account the ergotropy extraction provided by the different evolutions. For instance, consider the case of Figure 7, where $\omega_A = 1$, $\beta_A = 0.5$, $\beta_B = 4$ and ω_B is left free. Correspondingly, in Figure 16, we plot the signal-to-noise ratio (SNR) of the extracted work for each transformation in its ergotropic regime, together with the lower bound of Equation (2) (dotted lines). Firstly, note that the double swap violates the TUR even if we are far from the optimal conditions on the parameters maximizing the SNR. Second, the TUR is violated in both regimes where U_3 extracts the ergotropy ($\omega_B \in [1/8, 1/4] \cup [1/2, 1]$). Third, differently from what we found in the case of optimal conditions, U_2 and U_3 can achieve better SNRs than the standard swap U_1 where the ergotropy is extracted.

The standard TUR is not the only relevant lower bound which we show in Figure 16. The tightest TUR that cannot be violated by any time-symmetric process was found in Ref. [33] and, applied to the extracted work, reads

$$\frac{\text{var}(W)}{\langle W \rangle^2} \geq \text{csch}^2[g(\langle \Sigma \rangle / 2)] \tag{50}$$

where $g(x)$ is the inverse of the function $x \tanh(x)$. Therefore, we expect that neither U_1 nor U_2 can violate this TUR, while U_3 in principle can. This is what we see in Figure 16, where the dot-dashed lines correspond to the lower bound determined by Equation (50): the SNR identified by the double swap U_3 is the only one that can violate the tight TUR, also within its ergotropic regime.

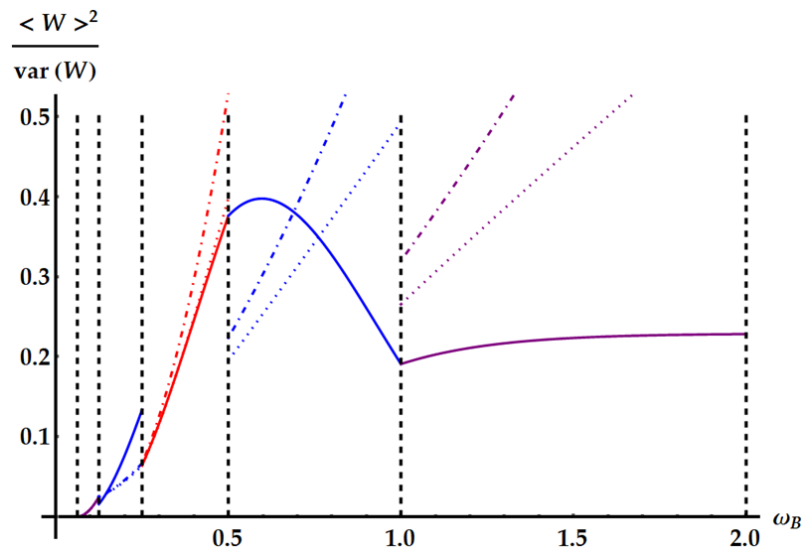


Figure 16. SNRs obtained from the ergotropy extraction of the example and parameters as in Figure (7). The vertical dashed lines separate different the ergotropic regimes. We have the idle swaps U_2 for $\omega_B \in [1/16, 1/8]$ and \tilde{U}_2 for $\omega_B \in [1, 2]$ (purple lines), the double swap U_3 for $\omega_B \in [1/8, 1/4]$ and for $\omega_B \in [1/2, 1]$ (blue lines) and U_1 for $\omega_B \in [1/4, 1/2]$ (red line). The solid curves display the SNR. The dotted and dot-dashed lines show the upper bounds provided by the standard TUR in Equation (2) and the tight TUR in Equation (50). In the region $\omega_B \in [1/2, 1]$, corresponding to the non-Hermitian unitary U_3 , strong violations of both TURs are apparent.

We focus more in detail on the violation of the TURs above in Figures 17–19, where we plot the SNRs for the three evolutions both for optimal values of the parameters independently from the ergotropy extraction and within the corresponding ergotropic regime. In particular, Figure 17 displays the performance of the standard swap U_1 . Here, we set $\beta_A \omega_A \ll 1$, which implies that the fluctuations are minimized for large $\beta_B \omega_B$. As $\beta_B \omega_B$ increases, the signal-to-noise ratio approaches the inverse of the minimal fluctuations, namely $3/2$, in agreement with Equation (43). Again, we find a slight violation of the standard TUR (dotted line).

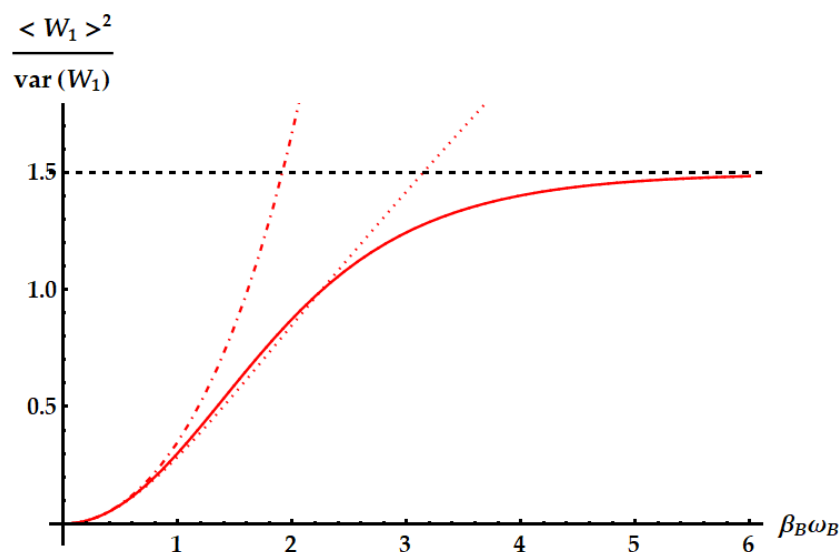


Figure 17. SNR of the work extracted by the standard swap U_1 (solid line) in ideal optimal conditions, with $\beta_A \omega_A = 10^{-3}$. The dotted and dot-dashed lines display the upper bound from the standard TUR in Equation (2) and the tight TUR in Equation (50), respectively. The dashed horizontal line highlights the asymptotic limit of the SNR.

In Figure 18, we show the performance of the idle swap U_2 where it maximizes the SNR (first panel) and extracts the ergotropy (second panel). Therefore, in the former case, we set $\beta_A \omega_A \ll 1$ and retrieve the optimization of the SNR for large values of $\beta_B \omega_B$, as in Equation (43). In the regime where U_2 extracts the ergotropy, as in Equation (44), we find an optimal SNR approaching 1/2 for $\beta_A \omega_A \gg \beta_B \omega_B \sim 0$ and an almost negligible violation of the standard TUR. Neither the standard nor the idle swap violates the tight TUR in Equation (50), displayed as a dashed-dotted line.

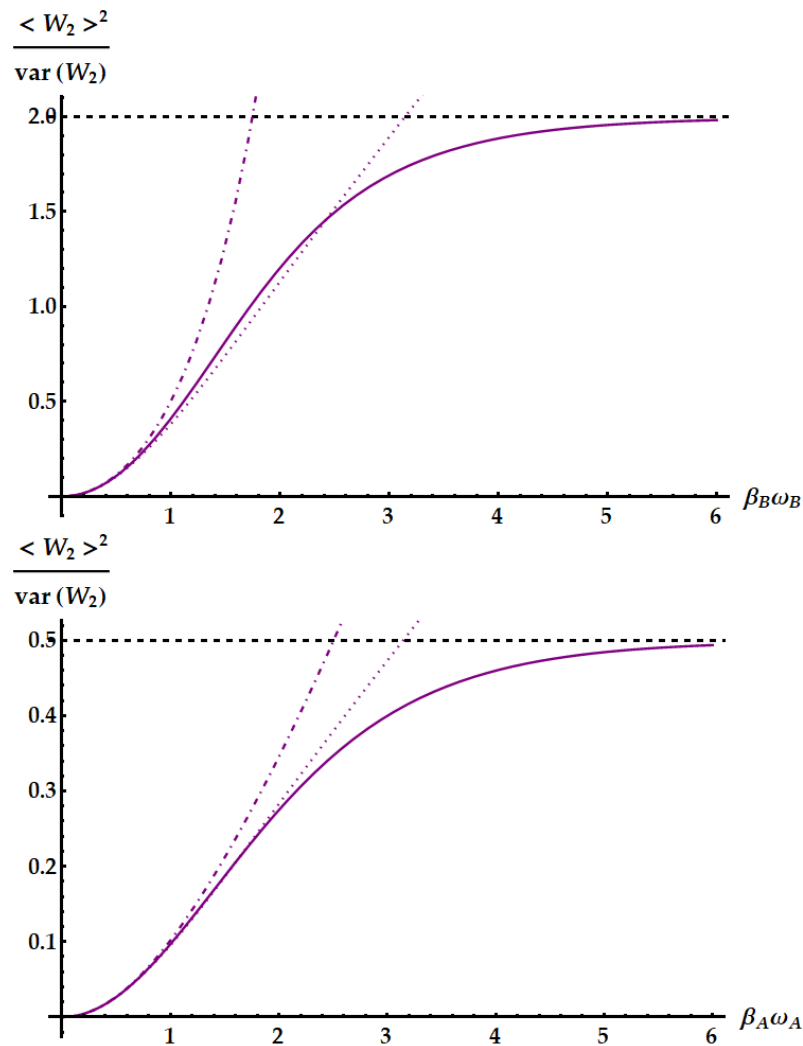


Figure 18. SNR of the work extracted by the idle swap U_2 (solid lines). The dotted lines display the upper bound from the standard TUR in Equation (2), while the dot-dashed lines display the upper bound from the tight TUR in Equation (50). The dashed horizontal lines highlight the limit of the SNR. **(Up panel):** conditions for the maximum SNR independently from the ergotropy extraction, namely $\beta_B \omega_B > \beta_A \omega_A \sim 0$. Here, we set $\beta_A \omega_A = 10^{-3}$. **(Bottom panel):** conditions for the maximum SNR within the ergotropic regime of U_2 , namely $\beta_A \omega_A > \beta_B \omega_B \sim 0$. Here we set $\beta_B \omega_B = 10^{-3}$.

The case of the double swap, displayed in Figure 19, is radically different. If we neglect the conditions for the ergotropy extraction, here we can optimize also over the frequency ratio ω_B/ω_A and we can set it to zero, while $\beta_A \omega_A \sim 0$, implying that we expect to find the optimal SNR for large $\beta_B \omega_B$, as in Equation (43). Again, the standard TUR is violated, but, compared with the previous cases, the corresponding bound is saturated for larger values of $\beta_B \omega_B$, where the SNR approaches its maximum. Most importantly, the tight TUR of Equation (50) is also violated, both when the SNR is optimized (first panel) and when the ergotropy is extracted (second panel).

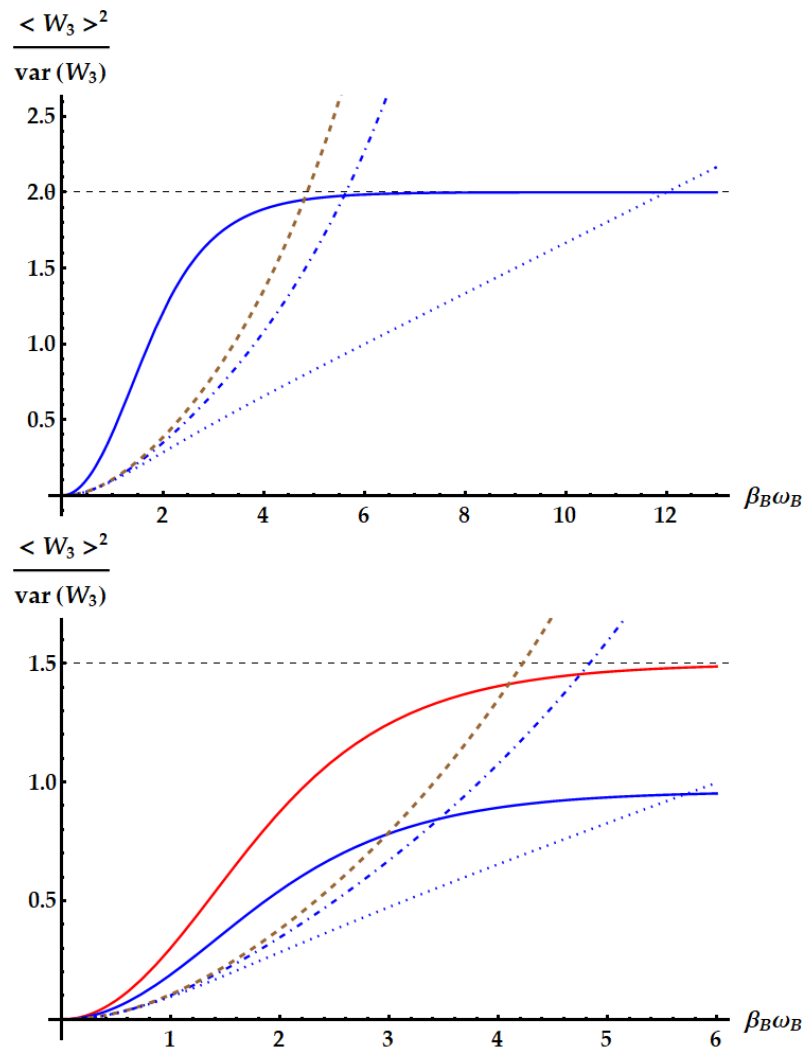


Figure 19. SNR of the work extracted by the double swap U_3 . The dotted and dot-dashed lines display the upper bound from the standard TUR in Equation (2) and the tight TUR in Equation (50). The dashed brown lines display the bound from the loosest TUR for time-symmetric processes in Equation (51). The dashed horizontal lines highlight the limit of the SNR. **(Up panel):** conditions for the maximum SNR independently from the ergotropy extraction, namely $\beta_B \omega_B > \beta_A \omega_A \sim 0$ and $\omega_B / \omega_A \sim 0$. Here, we set $\beta_A \omega_A = \omega_B / \omega_A = 10^{-3}$. The solid blue line displays the SNR. **(Bottom panel):** conditions for the maximum SNR within the ergotropic regime of U_3 , namely $\beta_B \omega_B > \beta_A \omega_A \sim 0$ and $\omega_B / \omega_A \in [1/2, 1]$. Here, we set $\beta_A \omega_A = 10^{-3}$ and show the cases obtained from two different choices of the frequency ratio. The red line displays the choice optimizing the SNR, i.e., $\omega_B / \omega_A = 1/2$, which reduces the statistics of the work extracted by the double swap to the one extracted by the standard swap. The blue solid line displays the case $\omega_B / \omega_A = 3/4$.

We also compare the SNR of U_3 with the loosest bound that always holds for time-symmetric processes [21,31,34] given by

$$\frac{\text{var}(W)}{\langle W \rangle^2} \geq \frac{2}{e^{\langle \Sigma \rangle} - 1}. \tag{51}$$

The bound from Equation (51) is displayed as a brown line in Figure 19. The violation that we find is a consequence of the fact that U_3 is not Hermitian.

In the second panel of Figure 19, as mentioned above, we explore the performance of the double swap U_3 in its ergotropic regime, where $\omega_B / \omega_A \in [1/2, 1]$. The best performance is obtained for $\omega_B / \omega_A = 1/2$, where the amount of work extracted by U_3 is the

same as the one extracted by U_1 (red line in Figure 19). We also plot the case $\omega_B/\omega_A = 3/4$, in blue. We obtain a worse SNR but still can observe a violation of all the TURs derived for time-symmetric processes.

The only TURs that can set a bound that cannot be violated by U_3 are those obtained without posing the symmetry between the forward and backward process. In fact, the TURs in Equations (50) and (51) have been generalized, respectively, in Refs. [32,39] by releasing the assumption that forward and backward processes share the same distribution of the stochastic variables. These new bounds are given by

$$\frac{\text{var}(W) + \text{var}(W)_B}{(\langle W \rangle + \langle W \rangle_B)^2} \geq \frac{1}{2} \text{csch}^2[g(a/2)] \tag{52}$$

and

$$\frac{\text{var}(W) + \text{var}(W)_B}{(\langle W \rangle + \langle W \rangle_B)^2} \geq \frac{1}{e^{a/2} - 1}, \tag{53}$$

where the quantities with subscript B are referred to the backward process and $a = (\langle \Sigma \rangle + \langle \Sigma \rangle_B)/2$. In the case of U_3 , the statistics of W for the backward process are easily found since $U_3^{-1} = \tilde{U}_3$. Hence, U_3^{-1} outputs the same work statistics as U_3 provided that systems A and B are swapped. Then, $\langle W_3 \rangle_B$, $\text{var}(W_3)_B$ and $\langle \Sigma_3 \rangle_B$ can be obtained from Equations (24), (28) and (42) simply swapping labels A and B . Note also that the bounds (right-hand sides) given by the TURs in Equations (52) and (53) depend only on the products $\beta\omega$, while the corresponding bounded quantities depend also on the frequency ratio ω_B/ω_A .

In Figure 20, we compare the reciprocal of the left-hand sides of Equations (52) and (53) for U_3 with the corresponding bounds as a function of $\beta_B\omega_B$ with fixed $\beta_A\omega_A \ll 1$. In this regime, U_3 maximizes the SNR. We show the two limiting cases $\omega_B/\omega_A \ll 1$ (thick dark-blue curve) and $\omega_B/\omega_A \gg 1$ (thin light-blue curve) together with the bounds obtained from the TURs in Equations (52) and (53), identified by the dot-dashed brown curve and the dashed green curve, respectively. Note that these TURs are never violated and, as expected, the first is tighter than the second. Having set $\beta_A\omega_A \sim 0$, the maximum is asymptotically reached for $\beta_B\omega_B \gg 1$ and $\omega_B \gg \omega_A$, and amounts to $8/9$ (dashed horizontal line in Figure 20).

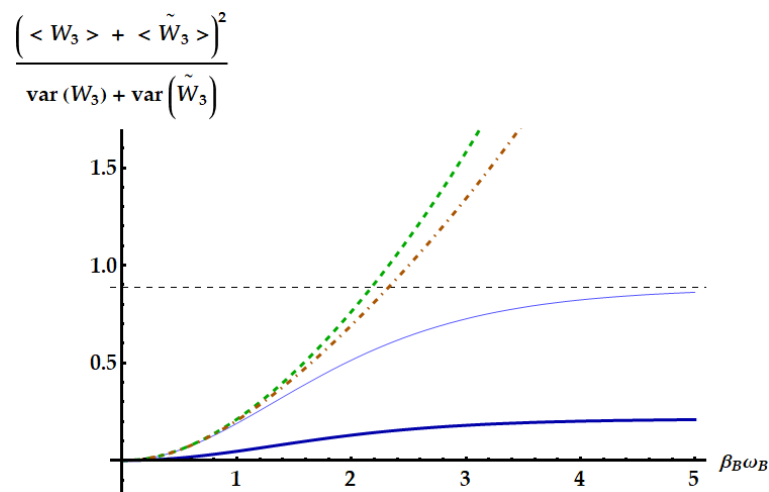


Figure 20. Ratio between the squared sum of the mean works extracted in the forward ($\langle W_3 \rangle$) and backward ($\langle \tilde{W}_3 \rangle$) processes and the sum of the corresponding variances as a function of $\beta_B\omega_B$ (solid lines). We set $\beta_A\omega_A = 10^{-3}$. We display the cases $\omega_B/\omega_A = 10^{-2}$ (dark-blue thick line) and $\omega_B/\omega_A = 10^2$ (light-blue thin line). The dot-dashed brown and the dashed green curve represent the upper bounds given by Equations (52) and (53), respectively. The dashed black horizontal line identifies the asymptotic value, which amounts to $8/9$ and is achieved for both $\beta_B\omega_B$, and $\omega_B/\omega_A \rightarrow \infty$.

4. Conclusions

We devised a consistent description of ergotropic heat engines for the optimal work extraction from a couple of quantum systems, which are cyclically restored to the canonical equilibrium at two different temperatures. We provided an exhaustive study for the case of two qutrits with equally-spaced energy levels by deriving the optimal ergotropic transformations, the statistics of the extracted work and the mean entropy production. We showed that going beyond the standard swap Otto engine allows one to improve the work extraction and also to enlarge the range of operation of the heat engine. We think that further interesting results for systems with arbitrary energy-level structures may be found by means of the approach outlined in Ref. [59]. Within the approach of stochastic thermodynamics we exploited a two-point measurement scheme to retrieve the first and second moment of the work distribution. We recall that, to this aim, many equivalent measurement schemes exist [60]. In future developments, it will be interesting to consider the effect of measurements explicitly performed on the quantum systems to monitor the engine, along with its impact on the thermodynamic cycles as performed, for example, in Ref. [61].

We focused on the relative fluctuations of the work extracted by each ergotropic transformation and showed that one of them, the double swap U_3 , violates many common TURs, specifically those based on the assumption that the distributions of the extracted work for the forward and backward processes are the same.

The application of our procedure to systems with higher dimensions is promising because it will lead to the generalization of the ergotropic transformations found for the qutrit case and will allow to finding new transformations which, as shown in this work, may possibly extract more work on average with lower fluctuations with respect to Otto engines based on the swap interaction with qudits.

Author Contributions: Conceptualization, M.F.S.; methodology, M.F.S.; validation, C.M.; formal analysis, G.C.; investigation, G.C. and M.F.S.; writing—original draft preparation, G.C.; writing—review and editing, C.M. and M.F.S.; visualization, C.M. and M.F.S.; supervision, C.M. and M.F.S.; project administration, C.M. and M.F.S.; funding acquisition, C.M. and M.F.S. All authors have read and agreed to the published version of the manuscript.

Funding: This research and the APC were funded by EU H2020 QuantERA ERA-NET Cofund in Quantum Technologies project QuICHE grant number 731473.

Data Availability Statement: Data sharing not applicable. No new data were created or analyzed in this study. Data sharing is not applicable to this article.

Acknowledgments: This material is based upon work supported the Italian MUR through PRIN 2022. C.M. acknowledges support from the PNRR MUR Project PE0000023-NQSTI.

Conflicts of Interest: The authors declare no conflict of interest. The funders had no role in the design of the study; in the collection, analyses, or interpretation of data; in the writing of the manuscript; or in the decision to publish the results.

Appendix A

Let us describe the two-stroke Otto engines. We consider two quantum systems A and B (with Hamiltonians H_A and H_B) initially at thermal equilibrium with their own reservoirs R_A and R_B (with Hamiltonians H_{R_A} and H_{R_B}) at inverse temperatures β_A and β_B . Without loss of generality, we take $\beta_A < \beta_B$. We assume weak coupling between systems and reservoirs so that we can represent the initial state as the tensor product of canonical density matrices, namely

$$\rho_0 \otimes \rho_R = \frac{1}{Z_A Z_B Z_{R_A} Z_{R_B}} e^{-\beta_A H_A} \otimes e^{-\beta_B H_B} \otimes e^{-\beta_A H_{R_A}} \otimes e^{-\beta_B H_{R_B}}, \quad (\text{A1})$$

where $Z_X = \text{Tr}[e^{-\beta_X H_X}]$. We perform a two-stroke cyclic heat engine by (i) isolating the two quantum systems from the reservoir at $t = 0^+$; (ii) extracting work by a unitary transformation U acting on the two systems up to time $t = \tilde{t}$; (iii) reconnecting the two quantum systems to their respective reservoirs by weak coupling to achieve complete thermalization at $t = t' \gg \tilde{t}$. We remark that the unitary U incorporates the free evolution of the two systems and their interaction obtained by external (possibly time-dependent) driving protocols, with the condition of being cyclic, namely, such that initial and final Hamiltonian coincide, i.e., $H_X = H_X(0) = H_X(\tilde{t})$ for both A and B .

The average value $\langle W \rangle$ of the work extracted on a cycle corresponds to the opposite of the variation of the internal energy of A and B during the unitary stroke U , i.e.,

$$\langle W \rangle = -\langle \Delta E_A \rangle - \langle \Delta E_B \rangle = \text{Tr}[(H_A + H_B)\rho_0] - \text{Tr}[(H_A + H_B)U\rho_0U^\dagger]. \tag{A2}$$

During the thermalization stroke, each system comes back to equilibrium, namely system A absorbs the average heat $\langle Q_H \rangle = \text{Tr}[H_A\rho_0] - \text{Tr}[H_AU\rho_0U^\dagger] = -\langle \Delta E_A \rangle$ from the hot reservoir, and system B dumps $\langle Q_C \rangle = \text{Tr}[H_B\rho_0] - \text{Tr}[H_BU\rho_0U^\dagger] = -\langle \Delta E_B \rangle$ on the cold one. In our convention the cycle operates as a heat engine when $\langle W \rangle > 0$, $\langle Q_H \rangle > 0$, and $\langle Q_C \rangle < 0$. Clearly, the first law is obtained as $\langle W \rangle = \langle Q_H \rangle + \langle Q_C \rangle$. At each cycle, the two quantum systems come back to their respective equilibrium states, and hence the average entropy production per cycle simply corresponds to $\langle \Sigma \rangle = -\beta_A \langle Q_H \rangle - \beta_B \langle Q_C \rangle = (\beta_A - \beta_B)\langle \Delta E_A \rangle - \beta_B \langle W \rangle$.

Let us now describe the above thermodynamical cycle by a set of stochastic trajectories which correctly reproduce the mean values of all thermodynamic variables by an average of stochastic variables over all possible trajectories. We adopt an operational approach based on complete energy measurements at different times [2,16,23] as in the typical derivation of Jarzynski equality [12]. This approach will allow us to study the complete statistics of work extraction and heat exchanges, and in particular to evaluate the fluctuations of work and their relation with entropy production.

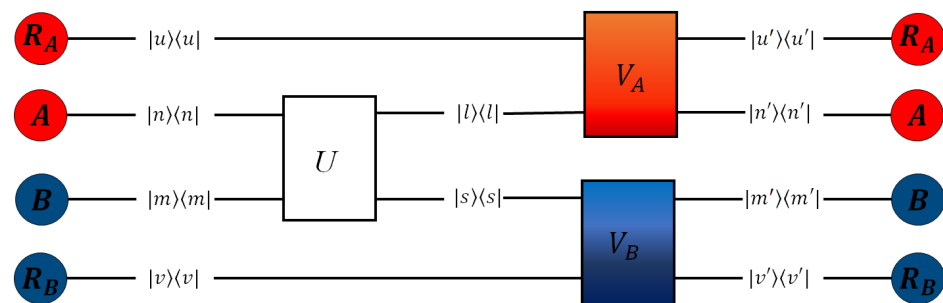


Figure A1. Scheme for the stochastic description of a cycle of the Otto two-stroke engine. Labels A and B identify the two systems operated by the engine as a working fluid, R_A and R_B are the corresponding reservoirs. The unitary U is the transformation extracting work, while V_A and V_B are the energy-preserving unitaries for the thermal relaxation of each system with its pertaining reservoir.

As depicted in Figure A1, we identify a single stochastic trajectory by the outcomes of the sequential fine-grained energy measurements of $H_A, H_B, H_{R_A}, H_{R_B}$ at the beginning of the cycle $t = 0^+$; of H_A, H_B at the end of the work stroke $t = \tilde{t}$ operated by U ; and finally of $H_A, H_B, H_{R_A}, H_{R_B}$ at the end of the thermalization stroke $t = t'$. We denote by V_X , with $X = A, B$, the unitary operator representing the joint evolution of system X and reservoir R_X by weak coupling and energy-preserving interaction up to complete thermal equilibrium at $t = t' \gg \tilde{t}$. By respecting the order of the above measurements, we denote by γ the stochastic trajectory corresponding to the sequence of outcomes, namely

$$\gamma = \{n, m, u, v; l, s; n', m', u', v'\} \tag{A3}$$

with corresponding energy eigenvalues

$$\{E_n^A, E_m^B, E_u^{R_A}, E_v^{R_B}; E_l^A, E_s^B; E_{n'}^A, E_{m'}^A, E_{u'}^{R_A}, E_{v'}^{R_B}\}. \tag{A4}$$

We could denote by $|i\rangle_C$ the eigenvector pertaining to the eigenvalue E_i^C of Hamiltonian H_C , with $C = A, B, R_A, R_B$, but we will generally write $|i\rangle$ instead of $|i\rangle_C$ since in the following it will be clear from the context (and with the help of Figure A1) the respective Hilbert space of all eigenvectors.

Let us now evaluate the probability $P[\gamma]$ of occurrence of a specific trajectory γ . Since the initial state is given by Equation (A1), the probability $p(n, m, u, v)$ for the initial outcomes n, m, u, v is given by the product of Gibbs weights, namely

$$p(n, m, u, v) = \frac{1}{Z_A Z_B Z_{R_A} Z_{R_B}} e^{-\beta_A(E_n^A + E_u^{R_A})} e^{-\beta_B(E_m^B + E_v^{R_B})}. \tag{A5}$$

The conditional probability $q_w(l, s|n, m)$ pertaining to the energy measurements of A and B with outcomes l and s after the unitary stroke U , given initial outcomes n and m , writes

$$q_w(l, s|n, m) = |\langle l|\langle s|U|n\rangle|m\rangle|^2. \tag{A6}$$

Finally, the conditional probability for the thermalization stage is given by

$$q_t(n', m', u', v'|l, s, u, v) = |\langle n'|\langle u'|V_A|l\rangle|u\rangle|^2 |\langle m'|\langle v'|V_B|s\rangle|v\rangle|^2. \tag{A7}$$

It follows that the probability of the trajectory $\gamma = \{n, m, u, v; l, s; n', m', u', v'\}$ is given by

$$P[\gamma] = p(n, m, u, v)q_w(l, s|n, m)q_t(n', m', u', v'|l, s, u, v). \tag{A8}$$

One easily identifies the functions of stochastic variables in correspondence to the thermodynamical variables of interest for each trajectory. Clearly, the work contribution corresponds to

$$W[\gamma] = E_n^A - E_l^A + E_m^B - E_s^B. \tag{A9}$$

On the other hand, the heat released by reservoirs A and B corresponds to

$$\begin{aligned} Q_H[\gamma] &= E_u^{R_A} - E_{u'}^{R_A} \simeq E_{n'}^A - E_l^A, \\ Q_C[\gamma] &= E_v^{R_B} - E_{v'}^{R_B} \simeq E_{m'}^B - E_s^B, \end{aligned} \tag{A10}$$

since we describe the thermalization with each reservoir by weak coupling and energy-preserving interactions [15]. Notice that under this approximation no work is generated by connecting and disconnecting the systems with the reservoirs [45,47,58].

By weighting each possible trajectory with its probability of occurrence we obtain the joint probability for extracting work W along with heat exchanges Q_H and Q_C as follows

$$\begin{aligned} p(W, Q_H, Q_C) &= \sum_{\gamma} P[\gamma] \delta(W - (E_n^A - E_l^A) - (E_m^B - E_s^B)) \\ &\times \delta(Q_H - (E_{n'}^A - E_l^A)) \delta(Q_C - (E_{m'}^B - E_s^B)). \end{aligned} \tag{A11}$$

Since V_X models the complete thermalization by the reservoir R_X , one has

$$\text{Tr}_{R_X} \left[V_X \left(\sigma \otimes \frac{1}{Z_{R_X}} e^{-\beta_X H_{R_X}} \right) V_X^\dagger \right] = \frac{1}{Z_X} e^{-\beta_X H_X} \tag{A12}$$

for arbitrary density matrix σ of system X . This fact can be used to simplify Equation (A11) by summing on all reservoir indexes $\{u, u', v, v'\}$. Hence, $p(W, Q_H, Q_C)$ can be rewritten in terms of measurements outcomes only on systems A and B , namely

$$p(W, Q_H, Q_C) = \sum_{n,m,l,s,n',m'} \frac{1}{Z_A^2 Z_B^2} e^{-\beta_A(E_n^A + E_{n'}^A) - \beta_B(E_m^B + E_{m'}^B)} |\langle l | \langle s | U | n \rangle | m \rangle|^2 \times \delta(W - (E_n^A - E_{l'}^A) - (E_m^B - E_{s'}^B)) \delta(Q_H - (E_{n'}^A - E_l^A)) \delta(Q_C - (E_{m'}^B - E_s^B)). \tag{A13}$$

Equation (A13) allows one to study the complete statistics of an ergotropic heat engine. The first principle of thermodynamics for the cycle is recovered since the average variation of the internal energy $\langle \Delta U \rangle = \langle Q_H + Q_C - W \rangle$ correctly gives zero, as shown as follows

$$\langle \Delta U \rangle = \langle Q_H + Q_C - W \rangle = \int dW \int dQ_H \int dQ_C p(W, Q_H, Q_C) (Q_H + Q_C - W) = \sum_{n,n',m,m'} \frac{1}{Z_A^2 Z_B^2} e^{-\beta_A(E_n^A + E_{n'}^A) - \beta_B(E_m^B + E_{m'}^B)} (E_{n'}^A - E_n^A + E_{m'}^B - E_m^B) = 0. \tag{A14}$$

One also has $\langle Q_H \rangle = -\langle \Delta E_A \rangle$, where $\langle \Delta E_A \rangle$ is the average variation of the internal energy of A during the unitary stroke, whose expectation can be obtained by averaging $E_l^A - E_n^A$ over all trajectories. Similarly, $\langle Q_C \rangle = -\langle \Delta E_B \rangle$, where $\langle \Delta E_B \rangle$ has corresponding stochastic values given by $E_s^B - E_{m'}^B$.

By introducing the trajectories for the thermalization stroke, we remark that the present result allows us to refine the approach of Refs. [33,35,36], where the stochastic values of Q_H were identified with $-\Delta E_A$ (and analogously for Q_C with $-\Delta E_B$). In fact, notice that the relation $W = Q_H + Q_C$ does not generally hold at the trajectory level. Anyway, since $\langle Q_H + \Delta E_A \rangle$ corresponds to the average of $E_{n'}^A - E_n^A$ over the trajectories, for increasing number of cycles the discrepancy between the stochastic variables Q_H and $-\Delta E_A$ remains bounded by the finite energy of system A , whereas both Q_H and ΔE_A increase linearly with the number of cycles, thus providing $\langle Q_H \rangle + \langle \Delta E_A \rangle = 0$. Analogous point applies for the variables Q_C and ΔE_B .

All results about the stochastic efficiency η of the heat engines given in Refs. [35,36] rigorously hold for η defined in terms of ΔE_A , namely $\eta = -W / \Delta E_A$. One could refine and compare the results for η defined as $\eta = W / Q_H$ by means of the probability distribution presented here in Equation (A13). The subtle difference between these two definitions of stochastic efficiency was already discussed in Ref. [45], where the thermalization in a two-stroke Otto engine was modeled by the quantum jump method.

The probability of work extraction is the marginal of $p(W, Q_H, Q_C)$ in Equation (A13) with respect to the heat exchanges, and one has

$$p(W) = \int dQ_H \int dQ_C p(W, Q_H, Q_C) = \sum_{n,m,l,s} \frac{1}{Z_A Z_B} e^{-\beta_A E_n^A - \beta_B E_m^B} |\langle l | \langle s | U | n \rangle | m \rangle|^2 \delta(W - (E_n^A - E_{l'}^A) - (E_m^B - E_{s'}^B)). \tag{A15}$$

Let us now consider a backward protocol where the measurements on the quantum systems and the reservoirs are performed in the reverse ordering, along with the time-reversal evolution of all interactions. The initial state for the backward protocol is again taken as the product of canonical density matrices, namely as in Equation (A1). By assuming that all Hamiltonians are invariant under time-reversal at all times [17,18,23], the backward protocol is then equivalent to follow Figure A1 from the right to the left, along with the replacement of V_A, V_B and U with V_A^\dagger, V_B^\dagger and U^\dagger , respectively.

We can compare the forward and the backward protocols by the probability $P[\gamma]$ of a trajectory $\gamma = \{n, m, u, v; l, s; n', m', u', v'\}$ and the probability $P_B[\gamma_B]$ for the occurrence of the specular reverse trajectory with the same measurement outcomes, namely $\gamma_B = \{n', m', u', v'; l, s; n, m, u, v\}$. The comparison between the forward and the backward

protocol is made by the logarithm of the probabilities, which defines the stochastic entropy $\Sigma[\gamma]$ generated along a trajectory γ as [18]

$$\Sigma[\gamma] = \log \frac{P[\gamma]}{P_B[\gamma_B]} . \tag{A16}$$

Since each γ identifies a corresponding backward trajectory γ_B , the fluctuation theorem simply follows as

$$\langle e^{-\Sigma} \rangle = \sum_{\gamma_B} P_B[\gamma_B] = 1 . \tag{A17}$$

In the present case, using Equation (A8) and the cancellation between forward and backward conditional probabilities for both q_w and q_t , one obtains

$$\frac{P[\gamma]}{P_B[\gamma_B]} = \frac{p(n, m, u, v)}{p(n', m', u', v')} , \tag{A18}$$

and hence

$$\begin{aligned} \Sigma[\gamma] &= \beta_A(E_{n'}^A - E_n^A + E_{u'}^{RA} - E_u^{RA}) + \beta_B(E_{m'}^B - E_m^B + E_{v'}^{RB} - E_v^{RB}) \\ &\simeq \beta_A(E_l^A - E_n^A) + \beta_B(E_s^B - E_m^B) , \end{aligned} \tag{A19}$$

where we used Equation (A10). As for the case of the stochastic work $W[\gamma] = E_n^A - E_l^A + E_m^B - E_s^B$, notice that also $\Sigma[\gamma]$ depends only on the reduced set of indexes $\{n, m, l, s\}$ pertaining to the unitary stroke operated by U . The probability of the stochastic entropy is then given by

$$p(\Sigma) = \sum_{n,m,l,s} \frac{1}{Z_A Z_B} e^{-\beta_A E_n^A - \beta_B E_m^B} |\langle l | \langle s | U | n \rangle | m \rangle|^2 \delta(\Sigma - \beta_A(E_n^A - E_l^A) - \beta_B(E_m^B - E_s^B)) . \tag{A20}$$

From Equation (A20), one correctly recovers the equivalent identities $\langle \Sigma \rangle = \beta_A \langle \Delta E_A \rangle + \beta_B \langle \Delta E_B \rangle = (\beta_A - \beta_B) \langle \Delta E_A \rangle - \beta_B \langle W \rangle = -\beta_A \langle Q_H \rangle - \beta_B \langle Q_C \rangle$.

Since from definition (A16) one has $\Sigma[\gamma_B] = -\Sigma[\gamma]$ we easily derive the detailed fluctuation theorem as follows

$$\begin{aligned} p(\Sigma) &= \sum_{\gamma} P[\gamma] \delta(\Sigma - \Sigma[\gamma]) = \sum_{\gamma} e^{\Sigma[\gamma]} P_B[\gamma_B] \delta(\Sigma - \Sigma[\gamma]) \\ &= e^{\Sigma} \sum_{\gamma} P_B[\gamma_B] \delta(\Sigma + \Sigma[\gamma_B]) = e^{\Sigma} p_B(-\Sigma) . \end{aligned} \tag{A21}$$

Indeed, by analogous derivation, for any set $\{X_i[\gamma]\}$ of odd stochastic variables such that $X_i[\gamma_B] = -X_i[\gamma]$, one has

$$p(\{X_i\}, \Sigma) = e^{\Sigma} p_B(\{-X_i\}, -\Sigma) . \tag{A22}$$

In particular, since $\Sigma = (\beta_A - \beta_B) \Delta E_A - \beta_B W$, we can also write [17,20,22,24]

$$\frac{p(W, \Delta E_A)}{p_B(-W, -\Delta E_A)} = e^{\Sigma} . \tag{A23}$$

where

$$\begin{aligned} p(W, \Delta E_A) &= \sum_{n,m,l,s} \frac{1}{Z_A Z_B} e^{-\beta_A E_n^A - \beta_B E_m^B} |\langle l | \langle s | U | n \rangle | m \rangle|^2 \\ &\times \delta(W - (E_n^A - E_l^A) - (E_m^B - E_s^B)) \delta(\Delta E_A - (E_l^A - E_n^A)) \end{aligned} \tag{A24}$$

and p_B identifies the distribution of the backward process, described by the transformation U^\dagger instead of U . We recall here that the relation $\Delta E_B = -W - \Delta E_A$ holds for the stochastic variables, namely at the trajectory level.

When the unitary operator U is of the form

$$U = e^{i\phi_A H_A + i\phi_B H_B} V e^{i\psi_A H_A + i\psi_B H_B}, \tag{A25}$$

with unitary Hermitian $V = V^\dagger$ and arbitrary phases $\phi_A, \phi_B, \psi_A, \psi_B$, notice that one has the symmetry

$$p_B(W, \Delta E_A) = p(W, \Delta E_A). \tag{A26}$$

Typically, this happens when the time-dependent protocol that actualizes the unitary evolution U is a time-symmetric driving [2,17,20]. We remark that the TUR in Equation (50) derived from the fluctuation theorem of Equation (A22) implicitly assumed the condition $p_B(\{X_i\}, \Sigma) = p(\{X_i\}, \Sigma)$.

Let us now consider in more detail the joint probability $p(W, \Delta E_A)$. The full statistics of W and ΔE_A is equivalently contained in the characteristic function $\chi(\lambda, \mu)$ given by the Fourier transform

$$\chi(\lambda, \mu) = \int dW \int d\Delta E_A p(W, \Delta E_A) e^{i\lambda W + i\mu \Delta E_A}. \tag{A27}$$

Here, λ and μ denote the counting parameters for W and ΔE_A , so that all moments and correlations can be recovered as

$$\langle W^j \Delta E_A^k \rangle = (-i)^{j+k} \left. \frac{\partial^{j+k} \chi(\lambda, \mu)}{\partial \lambda^j \partial \mu^k} \right|_{\lambda=\mu=0}. \tag{A28}$$

Using Equation (A24) and applying the delta functions in the integrals of Equation (A27) one obtains

$$\begin{aligned} \chi(\lambda, \mu) &= \frac{1}{Z_A Z_B} \sum_{n,m,l,s} e^{-\beta_A E_n^A} e^{-\beta_B E_m^B} e^{i\lambda(E_n^A - E_l^A + E_m^B - E_s^B)} e^{i\mu(E_l^A - E_n^A)} \\ &\times \text{Tr}[U^\dagger(|l\rangle\langle l| \otimes |s\rangle\langle s|) U(|n\rangle\langle n| \otimes |m\rangle\langle m|)] \\ &= \text{Tr}[U^\dagger(e^{-i(\lambda-\mu)H_A} \otimes e^{-i\lambda H_B}) U(e^{i(\lambda-\mu)H_A} \otimes e^{i\lambda H_B}) \rho_0]. \end{aligned} \tag{A29}$$

Recalling Equation (A1), one easily verifies the identity $\chi[-i\beta_B, i(\beta_A - \beta_B)] = 1$, which corresponds to the fluctuation theorem of Equation (A17). In fact, one has

$$\langle e^{-\Sigma} \rangle = \int dW \int \Delta E_A p(W, \Delta E_A) e^{\beta_B W - (\beta_A - \beta_B) \Delta E_A} = \chi[-i\beta_B, i(\beta_A - \beta_B)] = 1. \tag{A30}$$

In terms of the characteristic function, we notice that the detailed fluctuation theorem of Equation (A23) is translated into the symmetry

$$\chi_R(\lambda, \mu) = \chi[-i\beta_B - \lambda, i(\beta_A - \beta_B) - \mu]. \tag{A31}$$

In the presence of a symmetry in the unitary stroke achieved by U such that for a real $x \neq 0$ one has

$$[H_A + xH_B, U] = 0, \tag{A32}$$

from Equation (A29) one obtains the corresponding property

$$\chi(\lambda, \mu) = \chi((1-x)\lambda + x\mu, (1-x)\lambda + x\mu) = \chi(0, \mu - (1-x^{-1})\lambda), \tag{A33}$$

i.e., the characteristic function becomes a function of a single variable. It follows that $x\partial_\lambda\chi = (1-x)\partial_\mu\chi$, and from Equation (A28) one obtains the symmetry relations

$$\langle W^j \Delta E_A^k \rangle = \left(\frac{x}{1-x} \right)^k \langle W^{j+k} \rangle = \left(\frac{1-x}{x} \right)^j \langle \Delta E_A^{j+k} \rangle, \quad (\text{A34})$$

namely the stochastic variables W and ΔE_A are perfectly correlated. Moreover, since $\Delta E_B = -W - \Delta E_A$, one has $\langle \Delta E_A^k \rangle = (-x)^k \langle \Delta E_B^k \rangle$. It also follows that the average entropy is simply proportional to the average work, namely

$$\langle \Sigma \rangle = \frac{x\beta_A - \beta_B}{1-x} \langle W \rangle. \quad (\text{A35})$$

The effect of a strong symmetry as Equation (A32) can be seen directly on the joint probability $p(W, \Delta E_A)$. In fact, by using the last expression in Equation (A33) for $\chi(\lambda, \mu)$ in the inverse Fourier transform of Equation (A27), one easily obtains

$$p(W, \Delta E_A) = p(\Delta E_A) \delta(W + (1-x^{-1})\Delta E_A), \quad (\text{A36})$$

namely one has the perfect correlation $p(W|\Delta E_A) = \delta(W + (1-x^{-1})\Delta E_A)$. In this case, one also recognizes that the stochastic ΔE_A -efficiency defined as the ratio $\eta_{\Delta E_A} = \frac{W}{-\Delta E_A}$, is a self-averaging quantity and has no fluctuations, since $\eta_{\Delta E_A} = 1 - x^{-1}$. Interestingly, under full correlation between W and ΔE_A (and hence between W and Σ), in Ref. [62] it is shown that a general lower bound for the mean entropy $\langle \Sigma \rangle$ in terms of the asymmetry of the marginal work distribution $p(W)$ evaluated by the relative entropy $D(p(W)||p(-W))$ is saturated.

References

- Li, N.; Ren, J.; Wang, L.; Zhang, G.; Hänggi, P.; Li, B. Colloquium: Phononics: Manipulating heat flow with electronic analogs and beyond. *Rev. Mod. Phys.* **2012**, *84*, 1045–1066. [[CrossRef](#)]
- Seifert, U. Stochastic thermodynamics, fluctuation theorems and molecular machines. *Rep. Prog. Phys.* **2012**, *75*, 126001. [[CrossRef](#)] [[PubMed](#)]
- Benenti, G.; Casati, G.; Saito, K.; Whitney, R.S. Fundamental aspects of steady-state conversion of heat to work at the nanoscale. *Phys. Rep.* **2017**, *694*, 1–124. [[CrossRef](#)]
- Dubi, Y.; Di Ventra, M. Colloquium: Heat flow and thermoelectricity in atomic and molecular junctions. *Rev. Mod. Phys.* **2011**, *83*, 131–155. [[CrossRef](#)]
- Josefsson, M.; Svilans, A.; Burke, A.M.; Hoffmann, E.A.; Fahlvik, S.; Thelander, C.; Leijnse, M.; Linke, H. A quantum-dot heat engine operating close to the thermodynamic efficiency limits. *Nat. Nanotechnol.* **2018**, *13*, 920–924. [[CrossRef](#)]
- Ritort, F. Nonequilibrium Fluctuations in Small Systems: From Physics to Biology. *Adv. Chem. Phys.* **2008**, *137*, 31–123.
- Gnesotto, F.S.; Mura, F.; Gladrow, J.; Broedersz, C.P. Broken detailed balance and non-equilibrium dynamics in living systems: A review. *Rep. Prog. Phys.* **2018**, *81*, 066601. [[CrossRef](#)]
- Rao, R.; Esposito, M. Nonequilibrium Thermodynamics of Chemical Reaction Networks: Wisdom from Stochastic Thermodynamics. *Phys. Rev. X* **2016**, *6*, 041064. [[CrossRef](#)]
- Van Vu, T.; Saito, K. Thermodynamic Unification of Optimal Transport: Thermodynamic Uncertainty Relation, Minimum Dissipation, and Thermodynamic Speed Limits. *Phys. Rev. X* **2023**, *13*, 011013. [[CrossRef](#)]
- Gallavotti, G.; Cohen, E.G.D. Dynamical Ensembles in Nonequilibrium Statistical Mechanics. *Phys. Rev. Lett.* **1995**, *74*, 2694–2697. [[CrossRef](#)]
- Jarzynski, C. Equilibrium free-energy differences from nonequilibrium measurements: A master-equation approach. *Phys. Rev. E* **1997**, *56*, 5018–5035. [[CrossRef](#)]
- Jarzynski, C. Nonequilibrium Equality for Free Energy Differences. *Phys. Rev. Lett.* **1997**, *78*, 2690–2693. [[CrossRef](#)]
- Crooks, G.E. Nonequilibrium Measurements of Free Energy Differences for Microscopically Reversible Markovian Systems. *J. Stat. Phys.* **1998**, *90*, 1481–1487. [[CrossRef](#)]
- Piechocinska, B. Information erasure. *Phys. Rev. A* **2000**, *61*, 062314. [[CrossRef](#)]
- Jarzynski, C.; Wójcik, D.K. Classical and Quantum Fluctuation Theorems for Heat Exchange. *Phys. Rev. Lett.* **2004**, *92*, 230602. [[CrossRef](#)]
- Talkner, P.; Hänggi, P. The Tasaki–Crooks quantum fluctuation theorem. *J. Phys. A* **2007**, *40*, F569–F571. [[CrossRef](#)]

17. Andrieux, D.; Gaspard, P.; Monnai, T.; Tasaki, S. The fluctuation theorem for currents in open quantum systems. *New J. Phys.* **2009**, *11*, 043014. [[CrossRef](#)]
18. Esposito, M.; Harbola, U.; Mukamel, S. Nonequilibrium fluctuations, fluctuation theorems, and counting statistics in quantum systems. *Rev. Mod. Phys.* **2009**, *81*, 1665–1702. [[CrossRef](#)]
19. Esposito, M.; Van der Broeck, C. Three Detailed Fluctuation Theorems. *Phys. Rev. Lett.* **2010**, *104*, 090601. [[CrossRef](#)]
20. Campisi, M.; Talkner, P.; Hänggi, P. Fluctuation Theorems for Continuously Monitored Quantum Fluxes. *Phys. Rev. Lett.* **2010**, *105*, 140601. [[CrossRef](#)]
21. Merhav, N.; Kafri, Y. Statistical properties of entropy production derived from fluctuation theorems. *J. Stat. Mech.* **2010**, *12*, P12022. [[CrossRef](#)]
22. Sinitzyn, N.A. Fluctuation relation for heat engines. *J. Phys. A* **2011**, *44*, 405001. [[CrossRef](#)]
23. Campisi, M.; Hänggi, P.; Talkner, P. Quantum fluctuation relations: Foundations and applications. *Rev. Mod. Phys.* **2011**, *83*, 771–791. [[CrossRef](#)]
24. Campisi, M. Fluctuation relation for quantum heat engines and refrigerators. *J. Phys. A* **2014**, *47*, 245001. [[CrossRef](#)]
25. Hänggi, P.; Talkner, P. The other QFT. *Nat. Phys.* **2015**, *11*, 108–110. [[CrossRef](#)]
26. Vo, V.T.; Van Vu, T.; Hasegawa, Y. Unified approach to classical speed limit and thermodynamic uncertainty relation. *Phys. Rev. E* **2020**, *102*, 062132. [[CrossRef](#)] [[PubMed](#)]
27. Salazar, D.S.P. Bound for the moment generating function from the detailed fluctuation theorem. *Phys. Rev. E* **2023**, *107*, L062103. [[CrossRef](#)] [[PubMed](#)]
28. Mohanta, S.; Saha, M.; Venkatesh, B.P.; Agarwalla, B.K. Bounds on nonequilibrium fluctuations for asymmetrically driven quantum Otto engines. *Phys. Rev. E* **2023**, *108*, 014118. [[CrossRef](#)] [[PubMed](#)]
29. Barato, A.C.; Seifert, U. Thermodynamic Uncertainty Relation for Biomolecular Processes. *Phys. Rev. Lett.* **2015**, *15*, 158101. [[CrossRef](#)] [[PubMed](#)]
30. Gingrich, T.R.; Horowitz, J.M.; Perunov, N.; England, J.L. Dissipation Bounds All Steady-State Current Fluctuations. *Phys. Rev. Lett.* **2016**, *116*, 120601. [[CrossRef](#)]
31. Proesmans, K.; Van den Broeck, C. Discrete-time thermodynamic uncertainty relation. *Europhys. Lett.* **2017**, *119*, 20001. [[CrossRef](#)]
32. Potts, P.P.; Samuelsson, P. Thermodynamic uncertainty relations including measurement and feedback. *Phys. Rev. E* **2019**, *100*, 052137. [[CrossRef](#)] [[PubMed](#)]
33. Timpanaro, A.M.; Guarneri, G.; Goold, J.; Landi, G.T. Thermodynamic uncertainty relations from exchange fluctuation theorems. *Phys. Rev. Lett.* **2019**, *123*, 090604. [[CrossRef](#)] [[PubMed](#)]
34. Hasegawa, Y.; Van Vu, T. Fluctuation Theorem Uncertainty Relation. *Phys. Rev. Lett.* **2019**, *123*, 110602. [[CrossRef](#)]
35. Sacchi, M.F. Multilevel quantum thermodynamic swap engines. *Phys. Rev. A* **2021**, *104*, 012217. [[CrossRef](#)]
36. Sacchi, M.F. Thermodynamic uncertainty relations for bosonic Otto engines. *Phys. Rev. E* **2021**, *103*, 012111. [[CrossRef](#)]
37. Van Vu, T.; Saito, K. Thermodynamics of Precision in Markovian Open Quantum Dynamics. *Phys. Rev. Lett.* **2022**, *128*, 140602. [[CrossRef](#)]
38. Salazar, D.S.P. Thermodynamic uncertainty relations from involutions. *Phys. Rev. E* **2022**, *106*, L062104. [[CrossRef](#)]
39. Francica, G. Fluctuation theorems and thermodynamic uncertainty relations. *Phys. Rev. E* **2022**, *105*, 014129. [[CrossRef](#)]
40. Feldmann, T.; Geva, E.; Kosloff, R.; Salamon, P. Heat engines in finite time governed by master equations. *Am. J. Phys.* **1996**, *64*, 485–492. [[CrossRef](#)]
41. Rezek, Y.; Kosloff, R. Irreversible performance of a quantum harmonic heat engine. *New J. Phys.* **2006**, *8*, 83. [[CrossRef](#)]
42. Quan, H.T.; Liu, Y.; Sun, C.P.; Nori, F. Quantum thermodynamic cycles and quantum heat engines. *Phys. Rev. E* **2007**, *76*, 031105. [[CrossRef](#)] [[PubMed](#)]
43. Thomas, G.; Johal, R.S. Coupled quantum Otto cycle. *Phys. Rev. E* **2011**, *83*, 031135. [[CrossRef](#)] [[PubMed](#)]
44. Abah, O.; Roßnagel, J.; Jacob, G.; Deffner, S.; Schmidt-Kaler, F.; Singer, K.; Lutz, E. Single-Ion Heat Engine at Maximum Power. *Phys. Rev. Lett.* **2012**, *109*, 203006. [[CrossRef](#)]
45. Campisi, M.; Pekola, J.; Fazio, R. Nonequilibrium fluctuations in quantum heat engines: Theory, example, and possible solid state experiments. *New J. Phys.* **2015**, *17*, 035012. [[CrossRef](#)]
46. Peterson, J.P.S.; Batalhão, T.B.; Herrera, M.; Souza, A.M.; Sarthour, R.S.; Oliveira, I.S.; Serra, R.M. Experimental Characterization of a Spin Quantum Heat Engine. *Phys. Rev. Lett.* **2019**, *123*, 240601. [[CrossRef](#)]
47. Molitor, O.A.D.; Landi, G.T. Stroboscopic two-stroke quantum heat engines. *Phys. Rev. A* **2020**, *102*, 042217. [[CrossRef](#)]
48. Piccione, N.; De Chiara, G.; Bellomo, B. Power maximization of two-stroke quantum thermal machines. *Phys. Rev. A* **2021**, *103*, 032211. [[CrossRef](#)]
49. Gramajo, A.L.; Paladino, E.; Pekola, J.; Fazio, R. Fluctuations and stability of a fast-driven Otto cycle. *Phys. Rev. B* **2023**, *107*, 195437. [[CrossRef](#)]
50. Kuznetsova, E.I.; Yurischev, M.A.; Haddadi, S. Quantum Otto heat engines on XYZ spin working medium with DM and KSEA interactions: Operating modes and efficiency at maximal work output. *Quantum Inf. Proc.* **2023**, *22*, 192. [[CrossRef](#)]
51. Allahverdyan, A.E. Maximal work extraction from finite quantum systems. *EPL* **2004**, *67*, 565–571. [[CrossRef](#)]
52. Allahverdyan, A.E.; Johal, R.S.; Mahler, G. Work extremum principle: Structure and function of quantum heat engines. *Phys. Rev. E* **2008**, *77*, 041118. [[CrossRef](#)] [[PubMed](#)]

53. Andolina, G.M.; Keck, M.; Mari, A.; Campisi, M.; Giovannetti, V.; Polini, M. Extractable Work, the Role of Correlations, and Asymptotic Freedom in Quantum Batteries. *Phys. Rev. Lett.* **2019**, *122*, 047702. [[CrossRef](#)] [[PubMed](#)]
54. Francica, G.; Binder, F.C.; Guarnieri, G.; Mitchison, M.T.; Goold, J.; Plastina, F. Quantum Coherence and Ergotropy. *Phys. Rev. Lett.* **2020**, *125*, 180603. [[CrossRef](#)] [[PubMed](#)]
55. Biswas, T.; Łobjko, M.; Mazurek, P.; Jałowiecki, K.; Horodecki, M. Extraction of ergotropy: Free energy bound and application to open cycle engines. *Quantum* **2022**, *6*, 841. [[CrossRef](#)]
56. Salvia, R.; De Palma, G.; Giovannetti, V. Optimal local work extraction from bipartite quantum systems in the presence of Hamiltonian couplings. *Phys. Rev. A* **2023**, *107*, 012405. [[CrossRef](#)]
57. Mazzoncini, F.; Cavina, V.; Andolina, G.M.; Erdman, P.A.; Giovannetti, V. Optimal control methods for quantum batteries. *Phys. Rev. A* **2023**, *107*, 032218. [[CrossRef](#)]
58. De Chiara, G.; Landi, G.; Hewgill, A.; Reid, B.; Ferraro, A.; Roncaglia, A.J.; Antezza, M. Reconciliation of quantum local master equations with thermodynamics. *New J. Phys.* **2018**, *20*, 113024. [[CrossRef](#)]
59. Uzdin, R.; Rahav, S. Passivity Deformation Approach for the Thermodynamics of Isolated Quantum Setups. *PRX Quantum* **2021**, *2*, 010336. [[CrossRef](#)]
60. Allahverdyan, A.E. Nonequilibrium quantum fluctuations of work. *Phys. Rev. E* **2014**, *90*, 032137. [[CrossRef](#)]
61. Son, J.; Talkner, P.; Thingna, J. Monitoring Quantum Otto Engines. *PRX Quantum* **2021**, *2*, 040328. [[CrossRef](#)]
62. Campisi, M.; Buffoni, L. Improved bound on entropy production in a quantum annealer. *Phys. Rev. E* **2021**, *104*, L022102. [[CrossRef](#)] [[PubMed](#)]

Disclaimer/Publisher's Note: The statements, opinions and data contained in all publications are solely those of the individual author(s) and contributor(s) and not of MDPI and/or the editor(s). MDPI and/or the editor(s) disclaim responsibility for any injury to people or property resulting from any ideas, methods, instructions or products referred to in the content.